
Low-Dimensional Adaptation of Rectified Flow: A New Perspective through the Lens of Diffusion and Stochastic Localization

Saptarshi Roy Alessandro Rinaldo Purnamrita Sarkar

Department of Statistics and Data Science
University of Texas at Austin, TX, USA

Abstract

In recent years, Rectified flow (RF) has gained considerable popularity largely due to its generation efficiency and state-of-the-art performance. In this paper, we investigate the degree to which RF automatically adapts to the intrinsic low dimensionality of the support of the target distribution to accelerate sampling. We show that, using a carefully designed choice of the time-discretization scheme and with sufficiently accurate drift estimates, the RF sampler enjoys an iteration complexity of order $O(k/\varepsilon)$ (up to log factors), where ε is the precision in total variation distance and k is the intrinsic dimension of the target distribution. In addition, we show that the denoising diffusion probabilistic model (DDPM) procedure is equivalent to a stochastic version of RF by establishing a novel connection between these processes and stochastic localization. Building on this connection, we further design a stochastic RF sampler that also adapts to the low-dimensionality of the target distribution under milder requirements on the accuracy of the drift estimates, and also with a specific time schedule. We illustrate with simulations on the synthetic data and text-to-image data experiments the improved performance of the proposed samplers implementing the newly designed time-discretization schedules. Codes are available in <https://github.com/roysaptaumich/Low-dim-RF>

1. Introduction

In the past few years, Rectified flow or Flow matching (Liu, 2022; Lipman et al., 2022) has gained much attention due to its state-of-the-art generative performance across various modalities including image generation (Liu et al., 2024; Yan et al., 2024), audio generation (Wang et al., 2024; Liu et al., 2025a), and video generation (Chen et al., 2025; Liu et al., 2025b). The success of RF stems from two key factors: (1) RF is a deterministic ordinary differential equation (ODE) based sampler that is easier to simulate compared to other stochastic samplers, and (2) RF learns almost straight trajectories between source and target data distribution via multiple reflow steps which leads to faster sampling. However, RF still faces several challenges.

- The reflow process is computationally intensive as it requires a large number of generated pairs to model the target distribution.
- It is well known that the multiple reflow steps can quickly lead to performance degradation of the learned flow model (Zhu et al., 2024; Kim et al., 2025).

Therefore, *understanding and mitigating the learning error in the first reflow itself is extremely important* to improve generation quality. There has been prior works (Potaptchik et al., 2024; Azangulov et al., 2024; Huang et al., 2024; Li & Yan, 2024; Liang et al., 2025) that shows the low-dimensional adaptation of DDPM. Therefore, DDPM enjoys accelerated convergence to achieve improved sampling which is consistent with empirical findings even when the ambient dimension is very high. To the best of our knowledge such results are not currently present for RF models. A recent work by Lee et al.

. Correspondence to: Saptarshi Roy <saptarshi.roy@austin.utexas.edu>.

(2024) has empirically shown that a certain U-shaped time-discretization improves the generative quality of the first reflow model. However, theoretical understanding of such phenomenon remains elusive and necessitates in-depth investigation.

To this end, we make three key contributions in this paper:

1. We design a novel U-shaped time-discretization that provably allows any off-the-shelf pretrained RF sampler to *quickly achieve improved generation quality* by adapting to intrinsic low-dimensional structure of the target distribution. In particular, the RF sampler enjoys $O(k/\varepsilon)$ (upto log factors) iteration complexity, where ε is the precision of the generated samples in total variation distance and k is the intrinsic dimension of the target distribution.
2. We demonstrate that DDPM is equivalent to a stochastic version of RF (which we refer to as Stoc-RF) under a proper time change by establishing a novel connection between these processes and stochastic localization (Eldan, 2020), which has been recently shown to be provide a unifying and effective framework for representing and analyzing diffusion-based sampling processes (Benton et al., 2023; Montanari, 2023; El Alaoui & Montanari, 2022). This equivalence is convenient as it allows us to view Stoc-RF through the lens of well understood DDPM processes, which are known to adapt to the low-dimensional structure of the target distribution. In fact, our analysis shows that stochastic localization can be leveraged to provide a unified and convenient representation of a variety of sampling methods.
3. Using the connection between DDPM and Stoc-RF, we further design a stochastic RF sampler that provably also adapts to the low-dimensional structure of the target distributions under less stringent assumptions on the learned model. We illustrate the superior performance of this sampler with various simulations. This also addresses one of the open questions posed in the ICML tutorial talk Liu (2025).

Notation. Throughout the paper, with some abuse of notations, we will identify a probability distribution with its Lebesgue density, which we will assume exists unless otherwise noted. For a distribution (Lebesgue density) p , we write $\text{supp}(p)$ to denote the support of p . For a random variable X we use $\text{Law}(X)$ to denote its distribution. For two distributions P and Q on \mathbb{R}^d with Lebesgue densities p and q respectively, their total variation distance is denoted by $\text{TV}(p, q) := \sup_A |P(A) - Q(A)| = 1/2 \int_{\mathbb{R}^d} |p(x) - q(x)| dx$, where the supremum is over all Borel subsets of \mathbb{R}^d .

2. Background and Preliminaries

2.1. Rectified Flow

In this section, we briefly introduce the basics of Rectified flow, a generative model that transitions between two distributions p_0 and p_1 by solving ODEs. We refer the reader to Liu (2024; 2022) for an exhaustive treatment. Let $p_{\text{data}} := p_1 = \text{Law}(X_1)$ be the target data distribution on \mathbb{R}^d , the data generating distribution from which we would like to draw samples. The linear-interpolation process is defined by

$$X_t = tX_1 + (1 - t)X_0, \quad 0 \leq t \leq 1 \quad (1)$$

where p_0 is the *standard Gaussian* distribution. We will assume an independent initial coupling, i.e., $(X_0, X_1) \sim p_0 \otimes p_1$ and let $p_t = \text{Law}(X_t)$, for any $t \in [0, 1]$. The RF procedure is a deterministic sampler arising from an ODE with *drift (or velocity) function* $v : \mathbb{R}^d \times [0, 1] \rightarrow \mathbb{R}^d$ defined as the solution to the optimization problem

$$v = \arg \min_f \int \mathbb{E} \|X_1 - X_0 - f(X_t, t)\|_2^2 dt, \quad (2)$$

where the minimization is over all functions $f : \mathbb{R}^d \times [0, 1] \rightarrow \mathbb{R}^d$. For each t , The above objective in (2) is minimized at

$$(x, t) \mapsto v_t(x) := v(x, t) = \mathbb{E}[X_1 - X_0 \mid X_t = x]. \quad (3)$$

Under appropriate regularity conditions (investigated in Bansal et al., 2025; Mena et al., 2025), the ODE

$$dZ_t = v_t(Z_t) dt, \quad Z_0 \sim N(0, I_d) \quad (4)$$

satisfies the marginal preserving property, i.e., $\text{Law}(Z_t) = \text{Law}(X_t) = p_t$, owing to the Fokker-Planck equation

$$\frac{\partial p_t}{\partial t} + \nabla \cdot (v_t p_t) = 0.$$

Hence, ODE (4) can be used for sampling from the target distribution p_1 .

To implement this procedure, one faces two key challenges. First, given a sample from the target distribution p_1 , one has to estimate the drift function, which is naturally done by empirically minimizing the objective in (2) over a large and expressive function class (e.g., U-Net). Secondly, for sampling, one must rely on a time-discretization scheme of the ODE (4). One such scheme is the Eulerian update rule, which, for a given discretization of the time course in N intervals, with $0 = t_0 < t_1 < \dots < t_N = 1$, evaluates

$$Y_{t_{i+1}} = Y_{t_i} + \eta_i \hat{v}_{t_i}(Y_{t_i}); \quad \eta_i := t_{i+1} - t_i, \quad 0 \leq i \leq N - 1, \quad (5)$$

where $Y_0 \sim N(0, I_d)$ and $\hat{v}_t(\cdot)$ is the estimated velocity at time t . Let $\hat{p}_1 := \text{Law}(Y_1)$ denote the distribution of the final step. Other types of time discretized schemes of the ODE (4) can be chosen for the sampling step, and the resulting discretization errors impact the sampling fidelity differently. This has been the focus of a recent line of works (Benton et al., 2023; Chen et al., 2023; Li et al., 2024a;b; Huang et al., 2024; Liang et al., 2025) aimed at identifying time-discretized versions of DDPM and DDIM samplers to achieve tight convergence rates.

The velocity function. Before proceeding, we illustrate the connection between the velocity $v_t(x)$ and the score function $s_t(x) := \nabla \log p_t(x)$. Recall that $X_0 \sim N(0, I_d)$ and independent of $X_1 \sim p_1$. Therefore, Tweedie's formula (Efron, 2011; Meng et al., 2021) immediately yields $v_t(x) = \frac{x}{t} + \frac{(1-t)}{t} s_t(x)$. Thus, estimating v_t is essentially equivalent to estimating the score s_t for $t \in (0, 1)$.

2.2. Stochastic rectified flow (Stoc-RF)

Since the work of DDIM (Song et al., 2021a) and DDPM (Song et al., 2021b), it is well known that SDEs can be converted to ODEs to obtain deterministic samplers. Conversely, it is also possible to convert ODEs to its equivalent SDE form to obtain stochastic samplers. In fact, prior works (Albergo et al., 2023; Xue et al., 2024; Hu et al., 2025a) have shown that stochastic samplers typically enjoy better generation quality. One reason behind the inferior performance of deterministic samplers is the possibility of error accumulation during the sampling step along the discrete trajectories stemming from inaccurate velocity estimates. In other words, if Y_{t_i} differs significantly from Z_{t_i} for some t_i , then the Euler step (5) accumulates error due to inaccurate evaluation of $\hat{v}_{t_i}(Y_{t_i})$. Therefore, this can further reinforce the deviation in evaluating $Y_{t_{i+1}}$. A way to mitigate the compounding error from successive Euler steps is to introduce a stochastic Langevin correction at each step. Empirically, (Hu et al., 2025b) showed that the resulting stochastic RF samplers enjoy better text rendering quality over deterministic samplers. We further illustrate this point with Figure 1, showing that the ODE-based RF trajectories appear to generate more outliers compared to the SDE-based Stoc-RF sampler.

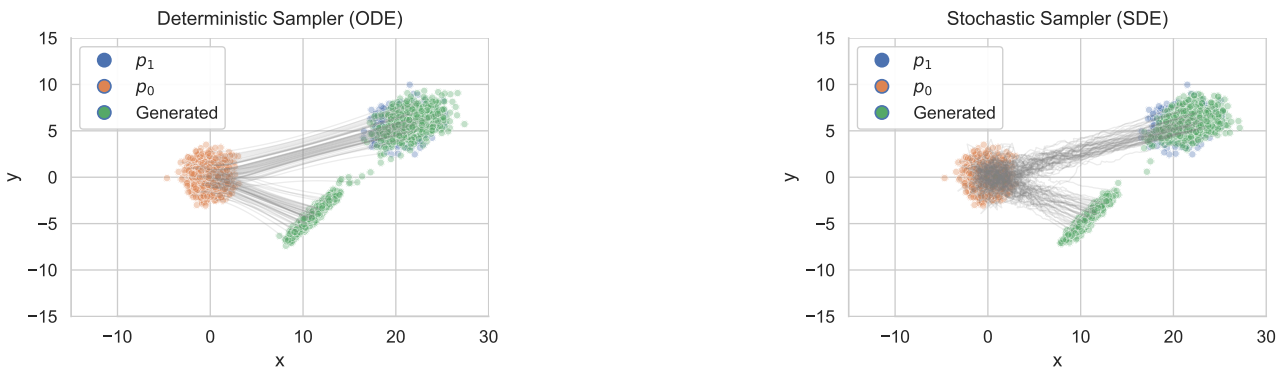


Figure 1. Trajectories of RF and Stoc-RF samplers for a mixture of 2-Gaussian target distribution.

Following e.g. Liu (2024, Chapter 5), the stochastic version of RF is specified by SDE

$$d\tilde{Z}_t = v_t(\tilde{Z}_t)dt + \underbrace{\gamma_t s_t(\tilde{Z}_t)dt + \sqrt{2\gamma_t} d\tilde{B}_t}_{\text{Langevin correction}}; \quad \tilde{Z}_0 = Z_0, \quad (6)$$

for $t \in [0, 1]$. This is obtained from adding a Langevin correction to the original RF ODE (4). Above, $\gamma_t \geq 0$ is a possibly time-varying diffusion coefficient, and $\{\tilde{B}_t\}_{t \geq 0}$ is the standard Brownian motion in \mathbb{R}^d . One can check (see, e.g., Liu (2024, Section 5.2) or Song et al. (2021b)) that the marginal $\tilde{p}_t := \text{Law}(\tilde{Z}_t)$ satisfies the continuity equation

$$\frac{\partial \tilde{p}_t}{\partial t} + \nabla \cdot (\tilde{v}_t \tilde{p}_t) = 0, \quad (7)$$

where $\tilde{v}_t(x) = v_t(x) + \gamma_t s_t(x) - \gamma_t \nabla \log \tilde{p}_t(x)$. Since the continuity equations (2.1) and (7) coincide, $\tilde{p}_t = p_t$, i.e., $\text{Law}(\tilde{Z}_t) = \text{Law}(Z_t)$, for all t , demonstrating that the SDE (6) can indeed be used for sampling from p_1 . In practice, this is accomplished via an appropriate time discretization scheme

$$\tilde{Z}_{t_{i+1}} = \tilde{Z}_{t_i} + \tilde{\eta}_i \left\{ v_{t_i}(\tilde{Z}_{t_i}) + \gamma_{t_i} s_{t_i}(\tilde{Z}_{t_i}) \right\} + \sqrt{2\tilde{\eta}_i \gamma_{t_i}} \xi_{t_i}, \quad (8)$$

where $\{t_i\}_{i=0}^N$ is an appropriate schedule of times, the ξ_{t_i} 's are i.i.d. draws from $N(0, I_d)$, and the $\tilde{\eta}_i$'s are (typically small) step-sizes. The Langevin term essentially acts as a course-corrector to the trajectory of (8) to adjust the trajectory distribution closer to p_t . Finally, one has freedom to choose the diffusion coefficients γ_t . In this paper we will restrict ourselves to the choice $\gamma_t = (1-t)/t$, which, as we will see below, is the *appropriate noise scaling that yields equivalence between the Stoc-RF SDE (6) and DDPM through the lens of Stochastic localization*. This also addresses an open question raised during the ICML tutorial talk Liu (2025) regarding the motivation of such choice.

3. Stochastic localization, and equivalence between RF and DDPM

Stochastic localization (SL). Stochastic localization is a probabilistic technique to investigate the properties of high-dimensional probability distributions due to (Eldan, 2020) that provides a powerful, unifying mathematical framework for understanding, analyzing, and improving score-based generative models and sampling algorithms. See El Alaoui & Montanari (2022), Montanari (2023) and the survey Shi et al. (2025), to which we refer the reader. To sample from the target data distribution p_1 , SL focusses on an appropriate measured-valued stochastic process $(\nu_s)_{s \geq 0}$ such that ν_s “localizes” towards p_1 as $s \rightarrow \infty$. A straightforward way to formulate this process is by letting, for any $s \geq 0$, $\nu_s := \text{Law}(X_1 | U_s)$, where $X_1 \sim p_1$ and

$$U_s = sX_1 + B_s, \quad (9)$$

with $(B_s)_{s \geq 0}$ a standard Brownian motion in \mathbb{R}^d (Montanari, 2023), independent of X_1 . Thus, ν_s is a random measure depending on U_s . Note that $U_s/s \rightarrow X_1$ almost surely as $s \rightarrow \infty$, i.e., ν_s does indeed localize around p_1 .

While enlightening, the construction (9) does not yield a sampler from p_1 , as it uses $X_1 \sim p_1$ in the definition of U_s . Towards that goal, it is instead convenient to consider the alternative process $(\tilde{U}_s)_{s \geq 0}$ defined as the solution of the SDE

$$d\tilde{U}_s = a_s(\tilde{U}_s) + d\tilde{B}_s, \quad (10)$$

where \tilde{B}_s is an independent Brownian motion and, for any $s \geq 0$, $a_s(u) = \mathbb{E}(X_1 | U_s = u)$. By classical SDE results – see Øksendal (Theorem 8.4.3 of 2003) or Liptser et al. (Theorem 7.12 of 2013) – $(U_s)_{s \geq 0}$ and $(\tilde{U}_s)_{s \geq 0}$ are equivalent in law. Therefore, (10) can be used for sampling from p_1 as long as we have access to the regression functions $\{a_s(\cdot), s \geq 0\}$, which can be estimated from the data. We also define the posterior covariance as $\mathbf{A}_s = \text{Cov}(X_1 | U_s)$. The next lemma from Eldan (2020) allows us to control the growth of the expected posterior covariance.

Lemma 3.1 (Eldan (2020), Equation (11)). *For all $s \geq 0$, $\frac{d}{ds} \mathbb{E}(\mathbf{A}_s) = -\mathbb{E}(\mathbf{A}_s^2)$.*

This is one of the crucial results that we will use later to control the discretization error of ODE and SDE samplers of RF.

SL and DDPM. DDPMs are a class of diffusion-based sampling mechanism for generative AI introduced by Ho et al. (2020). DDPM first starts with a *forward process* $(Y'_\tau)_{\tau \geq 0}$ starting from $Y'_0 = X_1 \sim p_1$ and evolving according to the SDE

$$dY'_\tau = -\beta(\tau) Y'_\tau d\tau + \sqrt{2\beta(\tau)} dB'_\tau, \quad Y'_0 \sim p_1, \quad (11)$$

where $\beta(\tau)$ is the diffusion coefficient and $\{B'_\tau\}_{\tau \geq 0}$ is standard Brownian motion. If $\beta(\tau) = 1$, then the SDE (11) reduces to the classical Ornstein-Uhlenbeck (OU) process. Typically, The forwards process is continued till a large time $\tau = N$ such that Y'_N is approximately Gaussian. Let $q_\tau(y'_\tau)$ be the marginals of y'_τ following (11). Then in order to sample from

the target distribution p_1 , a *reverse process* $(\overleftarrow{Y}_\tau)_{\tau \in [0, N]}$ is formulated, starting at $\overleftarrow{Y}_0 = Y'_N$ and evolving according to the reverse-time SDE

$$d\overleftarrow{Y}_\tau = \{\overleftarrow{Y}_\tau + 2\nabla \log q_{N-\tau}(\overleftarrow{y}_\tau)\} \beta(N-\tau) d\tau + \sqrt{2\beta(N-\tau)} dB_\tau, \quad (12)$$

where $(\overleftarrow{B}_\tau)_{\tau \geq 0}$ is a standard Brownian motion. Classical results in SDE (Anderson, 1982; Haussmann & Pardoux, 1986) show that $\overleftarrow{Y}_\tau \stackrel{d}{=} Y'_{N-\tau}$ which allows us to generate samples from p_1 via simulating the backward SDE (12).

It is known that DDPMs and stochastic localization are equivalent (Montanari, 2023). In particular, Benton et al. (2023) showed that the forward process (11) is *equivalent in law* to the SL process (9) under an appropriate time change. In this section, we restate this result in a slightly different fashion that will allow us to easily see the connection between DDPM and RF. To this end, we define $\omega_\tau := \exp(-2 \int_0^\tau \beta(u) du)$. Then the following lemma shows that the the *forward process* (11) and the SL process (9) are equivalent:

Lemma 3.2. *Let $\{\tau(s)\}_{s \geq 0}$ be sequence such that $\frac{1-\omega_{\tau(s)}}{\omega_{\tau(s)}} = \frac{1}{s}$. Then, we have $\left\{ \frac{Y'_{\tau(s)}}{\sqrt{\omega_{\tau(s)}}} \right\}_{s \geq 0} \stackrel{d}{=} \left\{ \frac{U_s}{s} \right\}_{s \geq 0}$.*

If $\beta(\tau) = 1$ for all τ (OU process), then the time transformation in Lemma 3.2 simplifies to be $\tau(s) = \frac{1}{2} \log(1 + s^{-1})$, and we get $\left\{ \frac{Y'_{\tau(s)}}{e^{-\tau(s)}} \right\}_{s \geq 0} \stackrel{d}{=} \left\{ \frac{U_s}{s} \right\}_{s \geq 0}$. Note, this matches the findings in Benton et al. (2023, Section 1.2). The proof is deferred to Appendix C.1.

SL, RF and Stoc-RF. Next, we will also show that the probability path of RF is also equivalent to the SL process (9). Recall that that RF starts by constructing the linear process $X_t = tX_1 + (1-t)X_0$, where $X_1 \sim p_1, X_0 \sim N(0, I_d)$ and $t \in [0, 1]$. To this end, we consider the process

$$\tilde{X}_t = tX_1 + tW_{(1-t)^2/t^2}, \quad t \in [0, 1] \quad (13)$$

where $(W_\tau)_{\tau \geq 0}$ is a Brownian motion. Note that $\text{Law}(\tilde{X}_t) = \text{Law}(X_t)$, for all $t \in [0, 1]$. In fact, as the next result show, the entire process (13) has the same law of the SL process (9), up to time-change.

Lemma 3.3. *Let $\{t(s)\}_{s \geq 0}$ be a sequence such that $\left(\frac{1-t(s)}{t(s)} \right)^2 = \frac{1}{s}$. Then, we have $\left\{ \frac{\tilde{X}_{t(s)}}{t(s)} \right\}_{s \geq 0} \stackrel{d}{=} \left\{ \frac{U_s}{s} \right\}_{s \geq 0}$.*

The proof is deferred to Appendix C.1. In light of Lemma 3.2 and Lemma 3.3, we immediately conclude that

$$\left\{ \frac{Y'_\tau}{\sqrt{\omega_\tau}} \right\}_{\tau \geq 0} \stackrel{d}{=} \left\{ \frac{\tilde{X}_{t(\tau)}}{t(\tau)} \right\}_{\tau \geq 0}, \quad (14)$$

where $t(\tau) = \frac{\sqrt{\omega_\tau}}{\sqrt{\omega_\tau} + \sqrt{1-\omega_\tau}}$. In fact, under the same time-change the Stoc-RF process (6) and the backward process (12) are equivalent.

Proposition 3.4. *Let $t(\tau) = \frac{\sqrt{\omega_\tau}}{\sqrt{\omega_\tau} + \sqrt{1-\omega_\tau}}$, and $\{\tilde{Z}_t\}_{t \geq 0}$ be a solution to the SDE (6). Then, $\left\{ \frac{\sqrt{\omega_{N-\tau}} \tilde{Z}_{t(N-\tau)}}{t(N-\tau)} \right\}_{\tau \geq 0}$ is a solution to the SDE (12). Conversely, if \overleftarrow{Y}_τ is a solution of SDE (12), then $\left\{ \frac{\overleftarrow{Y}_{\tau(t)}}{\sqrt{\omega_{N-\tau(t)}} + \sqrt{1-\omega_{N-\tau(t)}}} \right\}_{\tau \geq 0}$ is a solution of SDE (6), where $\tau(t)$ is the unique solution of the integral equation $\int_0^{N-\tau} \beta(u) du = \log \left(\sqrt{1 + \frac{(1-t)^2}{t^2}} \right)$.*

The above proposition is very useful in analyzing the convergence rate of Stoc-RF. Essentially, Proposition 3.4 allows us to transit between DDPM and Stoc-RF under simple time change and scaling. Therefore, convergence properties of one process can be carried over to the other one with the same transformation. This is the key insight that we will use to prove our convergence result of Stoc-RF in later sections. The detailed proof is deferred to Appendix C.2.

SL and Stochastic Interpolants. Lemma 3.3 and the equivalence result in (14) can be extended to cover general stochastic interpolation (Albergo & Vanden-Eijnden, 2023) schemes beyond RF. In detail, instead of a linear interpolation, one can consider a general deterministic affine interpolation process $I_\theta = a_\theta X_1 + b_\theta X_0$, where $a_{(\cdot)}$ and $b_{(\cdot)}$ are smooth functions of $\theta \in [0, 1]$, with $a_0 = b_1 = 0$, and $a_1 = b_0 = 1$. When $X_0 \sim N(0, I_d)$, the associated stochastic interpolant is the process

$(\tilde{I}_\theta)_{\theta \in [0,1]}$, where $\tilde{I}_\theta = a_\theta X_1 + a_\theta W_{r_\theta^2}$, with $r_\theta = b_\theta/a_\theta$ and $\{W_t\}_{t \geq 0}$ a Brownian motion. It is easy to see that $\tilde{I}_\theta \stackrel{d}{=} I_\theta$, for each θ . Moreover, each stochastic interpolant can be rescaled and time-transformed to return the SL process, in a sense made precise by the next result.

Proposition 3.5. $\left\{ \frac{\tilde{I}_{\theta(s)}}{a_{\theta(s)}} \right\}_{s \geq 0} \stackrel{d}{=} \left\{ \frac{U_s}{s} \right\}_{s \geq 0}$, with $r_{\theta(s)}^2 = \frac{1}{s}$.

In particular, in virtue of Lemma 3.3, RF is equal in law to any interpolant process I_θ under the time change $t(\theta) = \frac{a_\theta}{a_\theta + b_\theta}$. This equivalence among stochastic interpolants is not new, as it has also been shown in Liu (2024) by direct arguments. Connection between diffusion and flow matching has also been studied in Albergo et al. (2023); Gao et al. (2024); Ma et al. (2024) through different perspectives. By leveraging the representation properties of the SL process, we establish this result in a more unified manner, which has the added benefit of directly applying to both stochastic interpolants and SDEs. The proof of Theorem 3.5 is deferred to Appendix C.3.

4. Main Results

In this section, we present our main convergence results for both deterministic and stochastic samplers. We begin by introducing and commenting on our key assumptions. Throughout, $\{t_i\}_{i=0}^N$ refers to the time schedule for both the RF and Stoc-RF procedures, as in (5) and (8), respectively, and N is the number of time steps.

4.1. Low-dimensionality of target distribution

To formalize the notion of low-dimensionality of the target data generating distribution p_1 , we turn to the geometric complexity of $\mathcal{X} := \text{supp}(p_1) \subseteq \mathbb{R}^d$ as measured by its metric entropy.

Assumption 4.1 (Low-dimensionality). Let $\epsilon_0 = N^{-c_{\epsilon_0}}$ for some sufficiently large $c_{\epsilon_0} > 0$. The ϵ_0 covering number of \mathcal{X} with respect to the Euclidean norm, $\mathcal{N}(\mathcal{X}, \|\cdot\|_2, \epsilon_0)$, satisfies

$$\log \mathcal{N}(\mathcal{X}, \|\cdot\|_2, \epsilon_0) \leq C_{\text{cover}} k \log N,$$

for some constant $C_{\text{cover}} > 0$ and integer k . The quantity k is referred as the intrinsic-dimension of \mathcal{X} .

The above assumption was introduced in recent works by Huang et al. (2024); Li & Yan (2024); Liang et al. (2025) on adaptation of diffusion methods to intrinsic low dimensionality of the target function. Notably, by increasing the number of steps N , the assumption is less and less stringent. Informally, Assumption 4.1 requires the support of p_1 to be concentrated *on or near* a k -dimensional set. The above definition of intrinsic dimension is fairly general, as it covers a variety of important low-dimensional structures. Examples satisfying Assumption 4.1 include k -dimensional linear subspace in \mathbb{R}^d and k -dimensional non-linear manifolds (provided \mathcal{X} is polynomially bounded as in Assumption 4.2). Structures with doubling-dimension k (Dasgupta & Freund, 2008; Kpotufe & Dasgupta, 2012) also satisfies Assumption 4.1. More detailed discussion on this can be found in Section 4.1.1 of Huang et al. (2024). Moreover, in practice, target distribution (e.g., image data) is supported on a lower dimensional manifold and the intrinsic dimension $k \ll d$ (Facco et al., 2017; Ansini et al., 2019; Pope et al., 2021).

Assumption 4.2 (Bounded support). There exists a universal constant $c_R > 0$ such that

$$\sup_{x \in \mathcal{X}} \|x\|_2 \leq R, \text{ where } R = N^{c_R}.$$

The bounded support assumption is not as stringent as it may appear at first, as the diameter of the support \mathcal{X} is allowed to scale polynomially (with arbitrarily large degree) in the number of iterations of the sampler, which accommodates a very wide range of practical applications, such as image generation.

4.2. Assumptions on velocity approximation error

Our next set of assumptions are concerned with the approximation error of the estimated velocity field \hat{v}_t and are also standard.

Assumption 4.3 (Velocity approximation). Define $(\varepsilon_i^v)^2 := \mathbb{E} \|v_{t_i}(X_{t_i}) - \hat{v}_{t_i}(X_{t_i})\|_2^2$. Then,

$$\frac{1}{N} \sum_{i=1}^N (\varepsilon_i^v)^2 \leq \varepsilon_v^2.$$

The above assumption essentially requires a good control on the mean-squared error of the estimated velocity field. Similar assumptions have been considered in (Bansal et al., 2025; Guan et al., 2025) to prove Wasserstein convergence of RF. In the context of score-matching algorithms, similar assumptions related to the score-approximation error have also appeared in prior works such as (Benton et al., 2023; Chen et al., 2023; Li et al., 2024b; Liang et al., 2025).

Finally, to derive convergence rates of the deterministic samplers of RF that are adaptive to the intrinsic dimension of the support of the target distribution, we require the velocity estimator \hat{v}_t to have higher order accuracy guarantees.

Assumption 4.4 (Higher-order approximations).

(a) Let $(\varepsilon_i^{J,1})^2 := \mathbb{E}\|\nabla v_{t_i}(X_{t_i}) - \nabla \hat{v}_{t_i}(X_{t_i})\|_F^2$. Then, $N^{-1} \sum_{i=1}^N (\varepsilon_i^{J,1})^2 \leq \varepsilon_{J,1}^2$. Also, we assume

$$\sup_{x \in \mathbb{R}^d} \eta_i \|\nabla v_{t_i}(x) - \nabla \hat{v}_{t_i}(x)\|_{\text{op}} \leq 1/8$$

for all $0 \leq i \leq N-2$.

(b) Let $(\varepsilon_i^{J,2})^2 := \mathbb{E}[\text{Tr}(\nabla v_{t_i}(X_{t_i}) - \nabla \hat{v}_{t_i}(X_{t_i}))^2]$. Then, $N^{-1} \sum_{i=1}^N (\varepsilon_i^{J,2})^2 \leq \varepsilon_{J,2}^2$.

(c) Let $(\varepsilon_i^H)^2 := \mathbb{E}\|\nabla \text{Tr}(\nabla v_{t_i}(X_{t_i}) - \nabla \hat{v}_{t_i}(X_{t_i}))\|_2^2$. Then, $N^{-1} \sum_{i=1}^N (\varepsilon_i^H)^2 \leq \varepsilon_H^2$.

Nearly identical assumptions have been used in Liang et al. (2025) in the context of DDIM. Intuitively, an adequate control of the higher-order approximation terms mitigates the propagation of error during sampling, as the deterministic samplers are unable to self-correct the path of the flow. In contrast, Assumption 4.4 is not required to prove convergence guarantees for Stoc-RF sampler as the Langevin term automatically acts as a path corrector term.

4.3. Convergence rate of rectified flow

In this section, we will establish the main convergence theorem for RF sampler (5), $Y_{t_{i+1}} = Y_{t_i} + \eta_i \hat{v}_{t_i}(Y_{t_i})$, $Y_0 \sim N(0, I_d)$.

Time partition. Our convergence guarantees for RF depend crucially on a carefully constructed U-shaped time schedule $\{t_i\}_{i=0}^N$, which we describe next. For given, user-specified values $h \in (0, 1)$ and $\delta \geq 0$, we consider the non-uniform time partition

$$t_j = \begin{cases} 0, & j = 0, \\ \delta, & j = 1, \\ (1+h)t_{j-1}, & 2 \leq j \leq \frac{N}{2}, \\ 1 - (1+h)(1-t_{j+1}), & \frac{N}{2} < j \leq N-2, \\ 1 - \delta, & j = N-1, \\ 1, & j = N. \end{cases} \quad (15)$$

We set h such that $t_{N/2} = \delta(1+h)^{(N-2)/2} = 1/2$. Using $N-2 > N/2$ (for $N > 4$), we arrive at

$$\frac{h}{2} \leq \log(1+h) = \frac{2 \log(\frac{1}{2\delta})}{N-2} \Rightarrow h \leq \frac{8 \log(\frac{1}{2\delta})}{N}. \quad (16)$$

We remark that the proposed time schedule is practicable, as it does not depend on any properties of p_1 . Typically, δ is chosen to be small, as this give rise to a U-shaped time discretization as shown in Figure 2. This type of choice is not unusual, as it yields more accurate estimates \hat{v}_t during training when $t \approx 0$ and $t \approx 1$. Prior empirical work by Lee et al. (2024) has shown that such U-shaped choice of partition results in better training of the RF model. Non-uniform time discretizations have also been considered by Huang et al. (2024); Li & Yan (2024); Liang et al. (2025) in the context DDPM and DDIM to establish low-dimensional adaptation of the models. It is important to emphasize that the specific peculiar form of the time schedule (15), while conforming to best empirical practices, is theoretically grounded, and it was derived directly as a result of our technical analysis of the RF dynamics (see Step 7 of the proof of Theorem 4.5, Appendix B.2). We are now ready to present the main convergence result for the RF sampler. The detailed proof of the result is deferred to Appendix B.2.

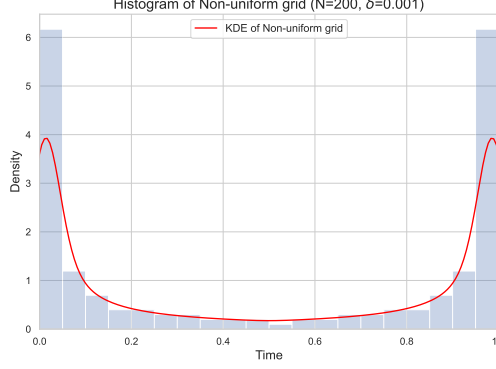


Figure 2. Histogram and kernel density estimation (KDE) plot of time-grid (15) showing U-shaped distribution.

Theorem 4.5. Let Assumptions 4.1-4.4 hold, and write $\mu_1 = \mathbb{E}_{X \sim p_1}[X]$. Let $\{Y_{t_i}\}_{i \geq 0}$ denote the RF updates of (5) with time schedule (15). Then, for $\delta = 1/(N \vee d)$, we have

$$\begin{aligned}
 & \text{TV}(p_{X_{t_{N-1}}}, p_{Y_{t_{N-1}}}) \\
 & \lesssim \frac{k \log^3(\frac{1}{\delta})}{N} + \frac{\log^2(\frac{1}{\delta})}{N} \varepsilon_{J,1}^2 + \frac{\log^2(\frac{1}{\delta})}{N} \varepsilon_v^2 \\
 & \quad + \log(1/\delta) (\varepsilon_v + \varepsilon_{J,1} + \varepsilon_{J,2} + \varepsilon_H) \\
 & \quad + \delta^2 \mathbb{E} \|X_1 - \mu_1\|_2^2 + \delta^2 (\varepsilon_0^v)^2 \\
 & \quad + \delta^2 (\varepsilon_0^{J,1})^2 + (\varepsilon_0^v + \varepsilon_0^{J,1} + \varepsilon_0^{J,2} + \varepsilon_0^H) + \delta^{-2} N^{-10}.
 \end{aligned} \tag{17}$$

Adaptation to low-dimensionality and accelerated convergence. The rate in Theorem 4.5 does not contain a direct dependence on the ambient dimension d and instead scales linearly in the intrinsic dimension k of \mathcal{X} , indicating that the RF sampler adapts to the low-dimensional structure of the target distribution. Thus, in principle, assuming perfect knowledge of the velocity drift (i.e. $\hat{v}_t = v_t$ and the higher approximation terms of Theorem 4.4 are all zero), the RF sampler (5) needs $\tilde{O}(k/\epsilon)$ iterations to achieve the guarantee $\text{TV}(p_{X_{t_{N-1}}}, p_{Y_{t_{N-1}}}) < \epsilon$. If the intrinsic dimension $k \ll d$, then the RF sampler automatically accelerates without any prior knowledge of the low-dimensionality of p_1 . To the best of our knowledge, this is the first work that provides a convergence guarantee of RF that adapts to the low-dimensionality of p_1 .

The dependence on $\mathbb{E} \|X_1 - \mu_1\|_2^2$. The upper bound in Theorem 4.5 contains a term involving $\mathbb{E} \|X_1 - \mu_1\|_2^2$, which even for data supported on manifolds would linearly in the ambient dimension d . However, in practice one can choose the free parameter δ to be e.g. $O(d^{-1})$, so that the term becomes negligible. With this choice of δ , last term in (17) scales as $d^2 N^{-10}$ which is also negligible in practice. For example, if $d = 256 \times 256$ and $N = 80$, then $d^2 N^{-10} \approx 4 \times 10^{-10}$.

Guarantee on perturbed data. The TV guarantee in Theorem 4.5 is on the penultimate update $Y_{t_{N-1}}$ of (5), and not on $Y_{t_N} = Y_1$. It is worthwhile to mention that $\text{TV}(p_{X_1}, p_{Y_{t_N}})$ might not be a useful or even meaningful quantity, as X_1 and Y_1 may have supports of different dimensions. For example, X_1 could be supported on a low-dimensional space, whereas Y_{t_N} would typically have full dimensional support, thereby rendering $\text{TV}(X_1, Y_{t_N}) = 1$. However, note that for any $\delta > 0$, $X_\delta \stackrel{d}{=} (1 - \delta)X_1 + \delta X_0$ has full-dimensional support due to the slight Gaussian perturbation. Therefore, the TV distance in Theorem 4.5 is well defined.

Higher-order approximation error terms. The upper bound in Theorem 4.5 is heavily dependent on the higher-order approximation errors of \hat{v}_t . As mentioned before, these terms are required to be small as deterministic samplers are unable to self-correct their trajectories. In addition, at $t = 0$, the true drift $v_0(x) = \mu_1 - x$ can be estimated by $\hat{v}_0(x) = n^{-1} \sum_{i \in [n]} X_1^{(i)} - x$, where $\{X_1^{(i)}\}_{i \in [n]} \stackrel{i.i.d.}{\sim} p_1$. With this choice of \hat{v}_0 , we have $\varepsilon_0^{J,1} = \varepsilon_0^{J,2} = \varepsilon_0^H = 0$, and $\varepsilon_0^v = \sqrt{\frac{\mathbb{E} \|X_1 - \mu_1\|_2^2}{n}}$.

4.4. Convergence rate of Stoc-RF

In this section, we will leverage the equivalence between DDPM and stoc-RF to design an SDE-based sampler that also adapts to the low-dimensionality of p_1 . We begin with the solution $\{Y'\}_{\tau \geq 0}$ to the forward process (11). We also consider the time-change map $\tau \in [0, \infty) \mapsto t(\tau) = \frac{\sqrt{\omega_\tau}}{\sqrt{\omega_\tau} + \sqrt{1 - \omega_\tau}}$. In light of (14) and Proposition 3.4, we note that $\{Y'_\tau\}_{\tau \geq 0}$ and $\{\tilde{Z}_t\}_{t \in [0, 1]}$ (recall (6)) are equivalent under the time change $\tau \mapsto t(\tau)$, and we have $\frac{Y'_\tau}{\sqrt{\omega_\tau}} \stackrel{d}{=} \frac{\tilde{Z}_{t(\tau)}}{t(\tau)}$.

In practice, we simulate the forward process by discretizing τ and setting specific values for ω_τ . In this section, we let $\omega_\tau = \prod_{j=1}^\tau \alpha_j$ with the α_j 's defined implicitly as

$$\begin{aligned} \beta_1 &:= 1 - \alpha_1 = \frac{1}{N^{c_0}}, \\ \beta_{\tau+1} &:= 1 - \alpha_{\tau+1} \\ &= \frac{c_1 \log N}{N} \min \left\{ \beta_1 \left(1 + \frac{c_1 \log N}{N} \right)^\tau, 1 \right\}, \quad 1 \leq \tau \leq N, \end{aligned} \tag{18}$$

for a user-specified choice of $c_0, c_1 > 0$. The time schedule above is very similar to the ones considered by Potapchik et al. (2024); Li et al. (2024b); Li & Yan (2024); Huang et al. (2024); Liang et al. (2025) to analyze the convergence properties of DDPM. Next, we recall the DDPM sampler considered in Liang et al. (2025); Huang et al. (2024); Li & Yan (2024):

$$\begin{aligned} \hat{Y}'_{\tau-1} &= \frac{1}{\sqrt{\alpha_\tau}} \left\{ \hat{Y}'_\tau + \delta_\tau \hat{s}_{Y'_\tau}(\hat{Y}'_\tau) + \nu_\tau \xi_\tau \right\}, \hat{Y}'_N \sim N(0, I_d) \\ \delta_\tau &= 1 - \alpha_\tau, \nu_\tau = \sqrt{\frac{(\alpha_\tau - \omega_\tau)(1 - \alpha_t)}{1 - \omega_\tau}}, \\ \tau &= N, N-1, \dots, 1, \quad \{\xi_\tau\}_{\tau \geq 1} \stackrel{i.i.d.}{\sim} N(0, I_d), \end{aligned} \tag{19}$$

and $\hat{s}_{Y'_\tau}$ is an approximate score of Y'_τ . The provide some intuition behind this sampler, we recall that $1 - \alpha_\tau = \beta_\tau \approx 0$. Hence, $1/\sqrt{\alpha_\tau} \approx 1 + \beta_\tau/2$, $\delta_\tau/\sqrt{\alpha_\tau} \approx \beta_\tau/2$, and $\nu_\tau/\sqrt{\alpha_\tau} \approx \sqrt{\beta_\tau}$. Substituting this in (19), we get

$$\hat{Y}'_{\tau-1} \approx \hat{Y}'_\tau + \frac{\beta_\tau}{2} \left\{ \hat{Y}'_\tau + 2\hat{s}_{Y'_\tau}(\hat{Y}'_\tau) \right\} + \sqrt{2 \cdot \left(\frac{\beta_\tau}{2} \right)} \xi_\tau, \tag{20}$$

which is essentially the discretized version of (12) with step-size $\beta_\tau/2$. Therefore, the sampler (19) roughly approximates the DDPM backward process.

Next, we convert (19) to a stoc-RF sampler using the equivalence between Y'_τ and $\tilde{Z}_{t(\tau)}$. To this end, we let, for any $t \in [0, 1]$, $\sigma_t^2 = (1 - t)^2 + t^2$, so that

$$\sigma_{t(\tau)}^2 = \frac{1}{(\sqrt{\omega(\tau)} + \sqrt{1 - \omega(\tau)})^2} = \frac{t^2(\tau)}{\omega_\tau}.$$

Therefore, we have $Y'_\tau \stackrel{d}{=} \tilde{Z}_{t(\tau)}/\sigma_{t(\tau)}$, and we have $s_{Y'_\tau}(y) = \sigma_{t(\tau)} s_{t(\tau)}(\sigma_{t(\tau)} y)$. We also define $t_i := t(N - i)$ for $i = 0, 1, \dots, N - 1$, and $R_i = t_i/\sigma_{t_i}$. Collecting everything above, an equivalent reformulation of (19) for RF sampling is

$$\begin{aligned} \frac{Y_{t_{i+1}}}{\sigma_{t_{i+1}}} &= \frac{R_{i+1}}{R_i} \left\{ \frac{Y_{t_i}}{\sigma_{t_i}} + \eta_i \sigma_{t_i} \hat{s}_{t_i}(Y_{t_i}) + \sqrt{\psi_i} W_{t_i} \right\}, \\ \frac{Y_{t_0}}{\sigma_{t_0}} &\sim N(0, I_d), \quad \{W_{t_i}\}_{i \geq 0} \stackrel{i.i.d.}{\sim} N(0, I_d), \\ i &= 0, 1, \dots, N - 1, \end{aligned} \tag{21}$$

where $\eta_i = 1 - \frac{R_i^2}{R_{i+1}^2}$, $\psi_i = \frac{R_i^2}{R_{i+1}^2} \cdot \frac{1 - R_{i+1}^2}{1 - R_i^2} \cdot \left(1 - \frac{R_i^2}{R_{i+1}^2} \right)$, and $\hat{s}_{t_i}(x) = \frac{t_i \hat{v}_{t_i}(x) - x}{1 - t_i}$. See Appendix B.3 for details. Lastly, we impose an assumption on the approximation error of \hat{s}_{t_i} .

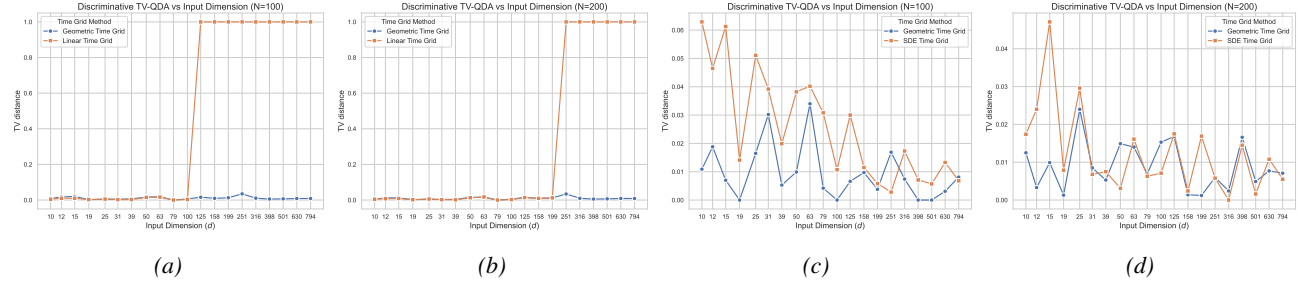


Figure 3. (a)-(b) TV distance between blurred low-rank Gaussian distribution and the generated samples by the RF sampler under uniform and non-uniform time-grid with varying d . (c)-(d) TV distance between blurred low-rank Gaussian distribution and the generated samples by the RF sampler under uniform and non-uniform time-grid with varying d .

Assumption 4.6. Define $(\varepsilon_i^s)^2 := \mathbb{E}\|s_{t_i}(X_{t_i}) - \hat{s}_{t_i}(X_{t_i})\|_2^2$. Then, we assume that $\frac{1}{N} \sum_{i=1}^N (\varepsilon_i^s)^2 \leq \varepsilon_s^2$.

Using the equivalence between (19) and (21), we obtain convergence guarantee for Stoc-RF, which the second main result of this paper.

Theorem 4.7. Under Assumption 4.1, 4.2 and 4.6, the stoc-RF sampler (21) satisfies

$$\text{TV}(Y_{t_{N-1}}, X_{t_{N-1}}) \lesssim \frac{k \log^3 N}{N} + \varepsilon_s \sqrt{\log N}.$$

Note that $t_{N-1} = \frac{\sqrt{\omega_1}}{\sqrt{\omega_1} + \sqrt{1-\omega_1}} \approx 1$. Therefore, $\text{Law}(X_{t_{N-1}}) \approx p_1$. In comparison with the results in Theorem 4.5, Stoc-RF sampler does not require any conditions on higher-order derivatives of the score or velocity field, as in Assumption 4.4. That is, Stoc-RF sampler can achieve similar performance under less stringent requirements. This is primarily due to the Gaussian perturbation term in (21) which acts as a corrector step. The proof is deferred to Appendix B.3.

Remark 4.8. Using the equivalence relation (14), one can also construct a deterministic RF sampler using the DDIM sampler considered in Liang et al. (2025, Theorem 1) and the same time change transformation considered in this section. The time schedule in this case also follows a U-shaped distribution, however, it is different from (15) (See Appendix B.4). One can show that the new sampler also adapts to the low-dimensionality of p_1 . However, we omit this discussion for brevity as the RF sampler in Theorem 4.5 already adapts to low-dimension with simpler time-steps.

5. Experiments

We have performed extensive simulations to corroborate our theoretical findings for both simulated data and real Text-to-Image (T2I) generation experiments.

5.1. Synthetic data experiments

In this section we demonstrate the usefulness of non-uniform time-grid for generation task from low-dimensional distribution. We set the intrinsic dimension $k = 8$, and set our target distribution to be $p_1 = N(\mu, \Sigma)$, where $\mu = (8, 8, \dots, 8)^\top \in \mathbb{R}^d$ and Σ is a block-diagonal matrix with blocks I_k and $\mathbf{0}_{(d-k) \times (d-k)}$. In this case, the drift $v_{t_i}(x)$ can be computed in closed form as

$$\begin{aligned} x \in \mathbb{R}^d \mapsto v_{t_i}(x) &= \frac{x}{t_i} + \frac{1-t_i}{t_i} s_{t_i}(x) \\ &= \begin{bmatrix} \frac{2t_i-1}{\sigma_{t_i}^2} I_k & \mathbf{0}_{k \times (d-k)} \\ \mathbf{0}_{(d-k) \times k} & -\frac{1}{1-t_i} I_{d-k} \end{bmatrix} x. \end{aligned} \tag{22}$$

In the experiments, we use (22) for generating new samples from p_1 . We vary the ambient dimension d between 10 and 800, and we let the number N of discretization-steps to be 100 and 200. We use both a non-uniform time-grid (15) (with $\delta = \min\{1/N, 1/d\}$) and a uniform time-grid for the generation task. We generate 2000 samples under the aforementioned discretization schemes and measure the TV distance with respect to another batch of 2000 samples independently generated

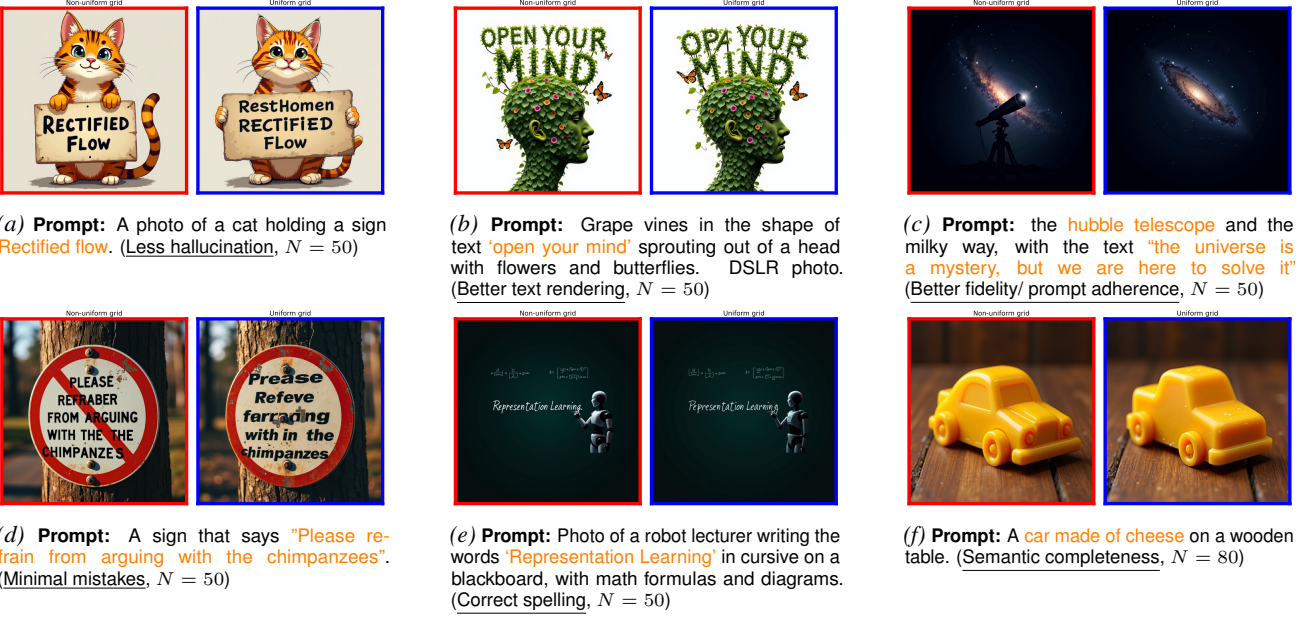


Figure 4. Generated images using Flux for specific prompts via Euler’s scheme (5) under non-uniform time-grid (15) (Red frame) and uniform time-grid (Blue frame).

from the slightly blurred target distribution $\text{Law}((1 - \delta)X_1 + \delta Z)$, where $Z \sim N(0, I_d)$. We use the discriminative approach proposed in Tao et al. (2024) to estimate the TV distance between the distributions via 10 independent Monte Carlo rounds. Figure 3(a)-(b) shows that nonuniform discretization has better adaptation to the low-dimensional structure of p_1 in high-dimensional regime.

For the SDE sampler (21), we also compare its TV convergence with that of the deterministic sampler (5) with the non-uniform time grid (15). Figure 3(c)-(d) shows that both sampler has similar performance across varying dimension.

Caution regarding approximation error. The TV convergence rate in both Theorems 4.5 and 4.7 depends highly on the approximation errors. In our experiments, we find that achieving good approximation error in high-dimensional regime is difficult even for the aforementioned simple low-dimensional Gaussian distribution case. We demonstrate this in a low-dimensional Gaussian example in Figure 6 where we set $k = 2$. The figure shows the generated data along the 3rd dimension for both the RF and Stoc-RF samplers. We can see that the growing dimension has an adverse effect on the generation quality. In fact, Stoc-RF appears to be more brittle, presumably due to its inherent stochasticity. The main difficulty in estimation stems from the non-smoothness of $v_t(\cdot)$ in (22) along the direction of low-dimensionality when $t \approx 1$. Such non-smoothness is hard to capture via the usual neural network class of functions (e.g., MLP, U-Net) that are typically smooth and necessitate the adoption of more expressive architecture. However, we postpone this direction to future research.

5.2. T2I experiments

We have performed various experiments to demonstrate the usefulness of the U-shaped time schedule (15) in the context of T2I. We use the Flux model (Labs, 2024; Labs et al., 2025) which is a pretrained RF model. For our experiments, we use the prompts designed by Liu et al. (2023); Hu et al. (2025b) to test and assess the generation quality. In these examples, we always set $\delta = 1/N$ for a specified choices of N . In Figure 4 we see that generation quality of RF is superior under a non-uniform time-grid (15) compared to uniform time-grid. In particular, the experiments indicate that a non-uniform grid helps to reduce hallucinations, enjoys better text rendering and achieves better semantic completeness.

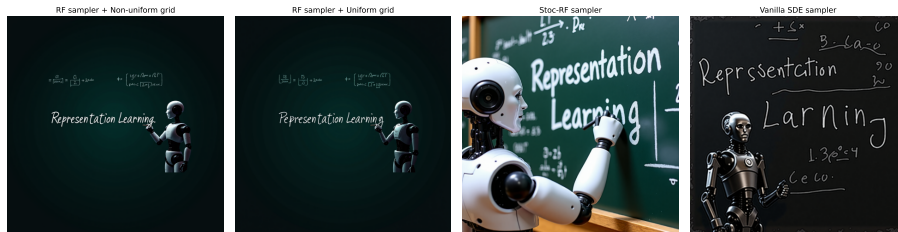
We also compare the generation quality of Stoc-RF sampler (21) and the vanilla SDE sampler (20) in Figure 5. The generated plots show that the quality is generally better for Stoc-RF sampler (21) compared to the RF sampler and the vanilla SDE sampler (20).



(a) **Prompt:** A photo of a cat holding a sign **Rectified flow**. ($N = 50$)



(b) **Prompt:** Grape vines in the shape of text ‘open your mind’ sprouting out of a head with flowers and butterflies. DSLR photo. ($N = 50$)



(c) **Prompt:** Photo of a robot lecturer writing the words ‘Representation Learning’ in cursive on a blackboard, with math formulas and diagrams. ($N = 50$)



(d) **Prompt:** A **car made of cheese** on a wooden table. ($N = 80$)

Figure 5. Generated images using Flux for specific prompts via Euler’s scheme (5) under non-uniform time-grid (15) (Columns 1), uniform time-grid (Column 2), Stoc-RF sampler (Column 3), and vanilla SDE sampler (Column 4). **Blue** color indicates the proposed methods in this paper. The generation quality of Stoc-Rf is generally better out of the four samplers.

6. Conclusions

In this paper, we design a new time-discretization scheme that allows any off-the-shelf pretrained RF sampler to achieve accelerated convergence by adapting to the low-dimensional structure of the target distribution. This allows the RF model to achieve better sampling quality in the first reflow step itself and also corroborates the empirical findings in Lee et al. (2024). Next, we show that the DDPM is equivalent to a stochastic version of RF by establishing a novel connection between these processes and the stochastic localization. Building on this connection, we further design a stochastic RF sampler that also adapts to the low-dimensionality of the target distribution under less stringent assumptions on the learned RF model.

References

Albergo, M. S. and Vanden-Eijnden, E. Building normalizing flows with stochastic interpolants. In *The Eleventh International Conference on Learning Representations*, 2023. URL <https://openreview.net/forum?id=li7qeBbCR1t>.

Albergo, M. S., Boffi, N. M., and Vanden-Eijnden, E. Stochastic interpolants: A unifying framework for flows and diffusions. *arXiv preprint arXiv:2303.08797*, 2023.

Alberts, T., Xu, Y., and Ye, Q. Joint stochastic localization and applications. *arXiv preprint arXiv:2505.13410*, 2025.

Anderson, B. D. Reverse-time diffusion equation models. *Stochastic Processes and their Applications*, 12(3):313–326, 1982.

Ansuini, A., Laio, A., Macke, J. H., and Zoccolan, D. Intrinsic dimension of data representations in deep neural networks. *Advances in Neural Information Processing Systems*, 32, 2019.

Azangulov, I., Deligiannidis, G., and Rousseau, J. Convergence of diffusion models under the manifold hypothesis in high-dimensions. *arXiv preprint arXiv:2409.18804*, 2024.

Bansal, V., Roy, S., Sarkar, P., and Rinaldo, A. On the wasserstein convergence and straightness of rectified flow. *arXiv preprint arXiv:2410.14949*, 2025. URL <https://arxiv.org/abs/2410.14949>.

Benton, J., De Bortoli, V., Doucet, A., and Deligiannidis, G. Nearly d -linear convergence bounds for diffusion models via stochastic localization. *arXiv preprint arXiv:2308.03686*, 2023.

Chen, S., Chewi, S., Li, J., Li, Y., Salim, A., and Zhang, A. R. Sampling is as easy as learning the score: theory for diffusion models with minimal data assumptions. In *The Eleventh International Conference on Learning Representations*, 2023.

Chen, S., Ge, C., Zhang, Y., Zhang, Y., Zhu, F., Yang, H., Hao, H., Wu, H., Lai, Z., Hu, Y., et al. Goku: Flow based video generative foundation models. In *Proceedings of the Computer Vision and Pattern Recognition Conference*, pp. 23516–23527, 2025.

Dasgupta, S. and Freund, Y. Random projection trees and low dimensional manifolds. In *Proceedings of the fortieth annual ACM symposium on Theory of computing*, pp. 537–546, 2008.

Efron, B. Tweedie’s formula and selection bias. *Journal of the American Statistical Association*, 106(496):1602–1614, 2011.

El Alaoui, A. and Montanari, A. An information-theoretic view of stochastic localization. *IEEE Transactions on Information Theory*, 68(11):7423–7426, 2022.

Eldan, R. Taming correlations through entropy-efficient measure decompositions with applications to mean-field approximation. *Probability Theory and Related Fields*, 176(3):737–755, 2020.

Facco, E., d’Errico, M., Rodriguez, A., and Laio, A. Estimating the intrinsic dimension of datasets by a minimal neighborhood information. *Scientific reports*, 7(1):12140, 2017.

Gao, R., Hoogeboom, E., Heek, J., Bortoli, V. D., Murphy, K. P., and Salimans, T. Diffusion meets flow matching: Two sides of the same coin. 2024. URL <https://diffusionflow.github.io/>.

Guan, Y., Balasubramanian, K., and Ma, S. Mirror flow matching with heavy-tailed priors for generative modeling on convex domains. *arXiv preprint arXiv:2510.08929*, 2025.

Haussmann, U. G. and Pardoux, E. Time reversal of diffusions. *The Annals of Probability*, pp. 1188–1205, 1986.

Ho, J., Jain, A., and Abbeel, P. Denoising diffusion probabilistic models. *Advances in neural information processing systems*, 33:6840–6851, 2020.

Hu, X., Liao, R., Xu, K., Liu, B., Li, Y., Ie, E., Fei, H., and Liu, Q. Improving rectified flow with boundary conditions. In *Proceedings of the IEEE/CVF International Conference on Computer Vision (ICCV)*, October 2025a. URL https://openaccess.thecvf.com/content/ICCV2025/papers/Hu_Improving_Rectified_Flow_with_Boundary_Conditions_ICCV_2025_paper.pdf.

Hu, X., Xu, K., Liu, B., Liu, Q., and Fei, H. Amo sampler: Enhancing text rendering with overshooting. In *Proceedings of the Computer Vision and Pattern Recognition Conference*, pp. 13157–13166, 2025b.

Huang, Z., Wei, Y., and Chen, Y. Denoising diffusion probabilistic models are optimally adaptive to unknown low dimensionality. *arXiv preprint arXiv:2410.18784*, 2024.

Kim, S. S., Kwon, M., Jeong, J., and Uh, Y. Balanced conic rectified flow. In *The Thirty-ninth Annual Conference on Neural Information Processing Systems*, 2025. URL <https://openreview.net/forum?id=kqHzgTV9AU>.

Kpotufe, S. and Dasgupta, S. A tree-based regressor that adapts to intrinsic dimension. *Journal of Computer and System Sciences*, 78(5):1496–1515, 2012.

Labs, B. F. Flux. <https://github.com/black-forest-labs/flux>, 2024.

Labs, B. F., Batifol, S., Blattmann, A., Boesel, F., Consul, S., Diagne, C., Dockhorn, T., English, J., English, Z., Esser, P., Kulal, S., Lacey, K., Levi, Y., Li, C., Lorenz, D., Müller, J., Podell, D., Rombach, R., Saini, H., Sauer, A., and Smith, L. Flux.1 kontext: Flow matching for in-context image generation and editing in latent space, 2025. URL <https://arxiv.org/abs/2506.15742>.

Lee, S., Lin, Z., and Fanti, G. Improving the training of rectified flows. *Advances in neural information processing systems*, 37:63082–63109, 2024.

Li, G. and Yan, Y. Adapting to unknown low-dimensional structures in score-based diffusion models. *Advances in Neural Information Processing Systems*, 37:126297–126331, 2024.

Li, G., Huang, Z., and Wei, Y. Towards a mathematical theory for consistency training in diffusion models. *arXiv preprint arXiv:2402.07802*, 2024a.

Li, G., Wei, Y., Chi, Y., and Chen, Y. A sharp convergence theory for the probability flow odes of diffusion models. *arXiv preprint arXiv:2408.02320*, 2024b.

Liang, J., Huang, Z., and Chen, Y. Low-dimensional adaptation of diffusion models: Convergence in total variation. *arXiv preprint arXiv:2501.12982*, 2025.

Lipman, Y., Chen, R. T., Ben-Hamu, H., Nickel, M., and Le, M. Flow matching for generative modeling. *arXiv preprint arXiv:2210.02747*, 2022.

Liptser, R., Aries, A., and Shiryaev, A. *Statistics of Random Processes I: General Theory*. Stochastic Modelling and Applied Probability. Springer New York, 2013. ISBN 9781475716658. URL <https://books.google.com/books?id=UavVBwAAQBAJ>.

Liu, H., Wang, J., Huang, R., Liu, Y., Lu, H., Zhao, Z., and Xue, W. Flashaudio: Rectified flow for fast and high-fidelity text-to-audio generation. In *Proceedings of the 63rd Annual Meeting of the Association for Computational Linguistics (Volume 1: Long Papers)*, pp. 13694–13710, 2025a.

Liu, J., Liu, G., Liang, J., Yuan, Z., Liu, X., Zheng, M., Wu, X., Wang, Q., Xia, M., Wang, X., et al. Improving video generation with human feedback. *arXiv preprint arXiv:2501.13918*, 2025b.

Liu, Q. Rectified flow: A marginal preserving approach to optimal transport, 2022. URL <https://arxiv.org/abs/2209.14577>.

Liu, Q. Let us flow together: Notes on rectified flow. https://www.cs.utexas.edu/~lqiang/PDF/flow_book.pdf, December 2024. Working Draft; version as of December 24, 2024.

Liu, Q. Flowing through continuous-time generative models: A clear and systematic tour. Tutorial presented at the 42nd International Conference on Machine Learning (ICML 2025), Vancouver, Canada, 2025. URL <https://icml.cc/virtual/2025/40011>.

Liu, R., Garrette, D., Saharia, C., Chan, W., Roberts, A., Narang, S., Blok, I., Mical, R., Norouzi, M., and Constant, N. Character-aware models improve visual text rendering. In *Proceedings of the 61st Annual Meeting of the Association for Computational Linguistics (Volume 1: Long Papers)*, pp. 16270–16297, 2023.

Liu, X., Zhang, X., Ma, J., Peng, J., et al. Instaflow: One step is enough for high-quality diffusion-based text-to-image generation. In *The Twelfth International Conference on Learning Representations*, 2024.

Ma, N., Goldstein, M., Albergo, M. S., Boffi, N. M., Vanden-Eijnden, E., and Xie, S. Sit: Exploring flow and diffusion-based generative models with scalable interpolant transformers. In *European Conference on Computer Vision*, pp. 23–40. Springer, 2024.

Mena, G., Kuchibhotla, A. K., and Wasserman, L. Statistical properties of rectified flow, 2025. URL <https://arxiv.org/abs/2511.03193>.

Meng, C., Song, Y., Li, W., and Ermon, S. Estimating high order gradients of the data distribution by denoising. *Advances in Neural Information Processing Systems*, 34:25359–25369, 2021.

Montanari, A. Sampling, diffusions, and stochastic localization. *arXiv preprint arXiv:2305.10690*, 2023.

Øksendal, B. Stochastic differential equations. In *Stochastic differential equations: an introduction with applications*, pp. 38–50. Springer, 2003.

Pope, P., Zhu, C., Abdelkader, A., Goldblum, M., and Goldstein, T. The intrinsic dimension of images and its impact on learning. *arXiv preprint arXiv:2104.08894*, 2021.

Potapchik, P., Azangulov, I., and Deligiannidis, G. Linear convergence of diffusion models under the manifold hypothesis. *arXiv preprint arXiv:2410.09046*, 2024.

Revuz, D. and Yor, M. *Continuous martingales and Brownian motion*, volume 293. Springer Science & Business Media, 2013.

Ruzhansky, M. and Sugimoto, M. On global inversion of homogeneous maps. *Bulletin of Mathematical Sciences*, 5(1): 13–18, 2015.

Shi, B., Tian, K., and Zhang, M. S. Perspectives on stochastic localization, 2025. URL <https://arxiv.org/abs/2510.04460>.

Song, J., Meng, C., and Ermon, S. Denoising diffusion implicit models. In *International Conference on Learning Representations*, 2021a. URL <https://openreview.net/forum?id=St1giarCHLP>.

Song, Y., Sohl-Dickstein, J., Kingma, D. P., Kumar, A., Ermon, S., and Poole, B. Score-based generative modeling through stochastic differential equations. In *International Conference on Learning Representations*, 2021b. URL <https://openreview.net/forum?id=PxTIG12RRHS>.

Tao, L., Xu, S., Wang, C.-H., Suh, N., and Cheng, G. Discriminative estimation of total variation distance: A fidelity auditor for generative data. *arXiv preprint arXiv:2405.15337*, 2024.

Wang, Y., Guo, W., Huang, R., Huang, J., Wang, Z., You, F., Li, R., and Zhao, Z. Frieren: Efficient video-to-audio generation network with rectified flow matching. *Advances in Neural Information Processing Systems*, 37:128118–128138, 2024.

Xue, K., Zhou, Y., Nie, S., Min, X., Zhang, X., Zhou, J., and Li, C. Unifying bayesian flow networks and diffusion models through stochastic differential equations. In *International Conference on Machine Learning*, pp. 55656–55681. PMLR, 2024.

Yan, H., Liu, X., Pan, J., Liew, J. H., Liu, Q., and Feng, J. Perflow: Piecewise rectified flow as universal plug-and-play accelerator. *arXiv preprint arXiv:2405.07510*, 2024.

Zhu, H., Wang, F., Ding, T., Qu, Q., and Zhu, Z. Analyzing and mitigating model collapse in rectified flow models. *arXiv preprint arXiv:2412.08175*, 2024.

A. Additional Figures

A.1. Comparison of generation quality of samplers with growing dimension

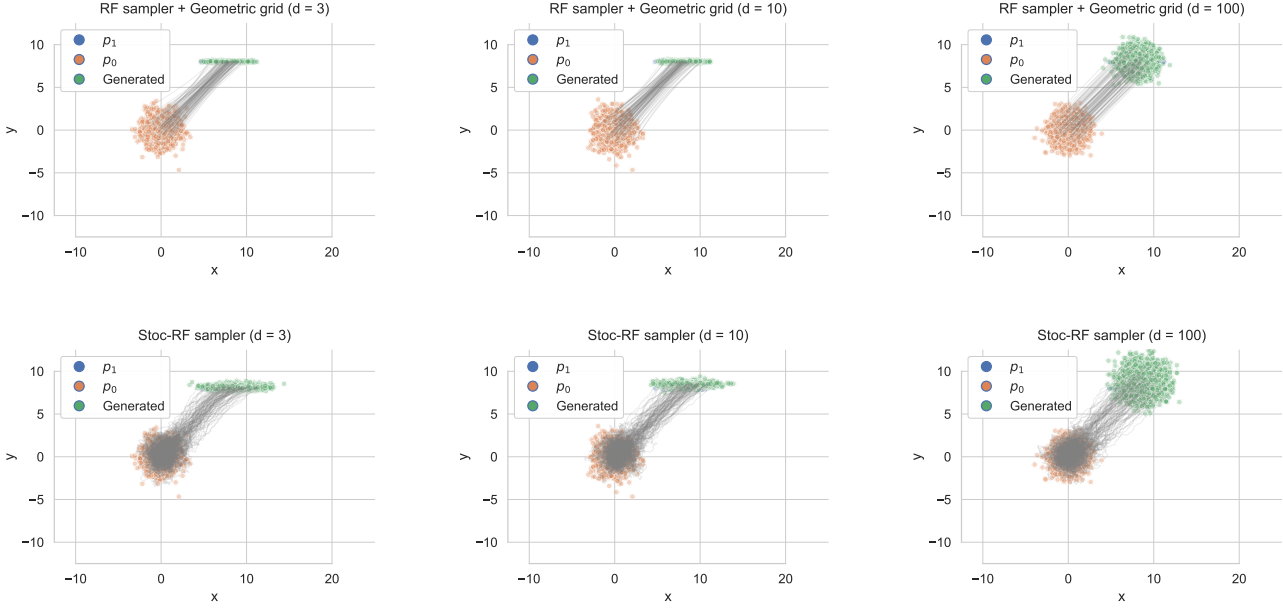


Figure 6. The generation quality of RF sampler and Stoc-RF sampler along the low-dimensional direction gradually degrades with growing dimension

B. Proof of main results

B.1. Velocity function and its first order identities

Before proceeding, we illustrate the connection between the velocity $v_t(x)$ and the score function $s_t(x) := \nabla \log p_t(x)$. To this end, we define two key quantities:

$$\mu_{1|t}(x) = \mathbb{E}[X_1 \mid X_t = x], \quad \text{Cov}_{1|t}(x) = \text{Cov}(X_1 \mid X_t = x).$$

With this, Equation (3) can be re-written as

$$v_t(x) = \mathbb{E}[X_1 - X_0 \mid X_t = x] = \frac{1}{1-t} (\mu_{1|t}(x) - x). \quad (23)$$

By the first and second order Tweedie's formula (Efron, 2011; Meng et al., 2021), it follows that, for any choice of $t \in (0, 1]$ and $x \in \mathbb{R}^d$,

$$\begin{aligned} \mu_{1|t}(x) &= \frac{x}{t} + \frac{(1-t)^2}{t} s_t(x), \\ \text{Cov}_{1|t}(x) &= \frac{(1-t)^2}{t^2} I_d + \frac{(1-t)^4}{t^2} \nabla s_t(x). \end{aligned}$$

Substituting this in (23), we obtain that

$$v_t(x) = \frac{x}{t} + \frac{(1-t)}{t} s_t(x), \quad \text{and} \quad \nabla v_t(x) = -\frac{I_d}{1-t} + \frac{t}{(1-t)^3} \text{Cov}_{1|t}(x).$$

B.2. Proof of convergence of RF sampler (Theorem 4.5)

Notational conventions. We begin with some notational conventions for the ease of presentation.

1. We define transition map for the Euler's scheme as

$$\Phi_{t_i}(x) := x + \eta_{t_i} \hat{v}_{t_i}(x) \quad \text{with } \eta_{t_i} = t_{i+1} - t_i,$$

where $\hat{v}_t(x)$ is the velocity estimate.

2. For notational brevity, we will use index i to denote the time t_i . In this index notation we have $X_N \equiv X_1 \sim p_1$
3. With the above notations in mind, we have

$$X_i = (1 - t_i)X_0 + t_i X_N, \quad \text{and} \quad Y_{i+1} = \Phi_i(Y_i). \quad (24)$$

Step 1: TV recursion. We start by obtaining a recursion relation between the TV distances between the updates Y_i and the ground truth X_i . For any $i \leq N - 2$, we have

$$\begin{aligned} \text{TV}(p_{X_{i+1}}, p_{Y_{i+1}}) &= \sup_{\mathcal{A} \subseteq \mathbb{R}^d} \{ \mathbb{P}_{X_{i+1}}(\mathcal{A}) - \mathbb{P}_{Y_{i+1}}(\mathcal{A}) \} = \sup_{\mathcal{A} \subseteq \mathbb{R}^d} \{ \mathbb{P}_{X_{i+1}}(\mathcal{A}) - \mathbb{P}_{Y_i}(\Phi_i^{-1}(\mathcal{A})) \} \\ &\leq \sup_{\mathcal{A} \subseteq \mathbb{R}^d} \{ \mathbb{P}_{X_{i+1}}(\mathcal{A}) - \mathbb{P}_{X_i}(\Phi_i^{-1}(\mathcal{A})) \} + \sup_{\mathcal{A} \subseteq \mathbb{R}^d} \{ \mathbb{P}_{X_i}(\Phi_i^{-1}(\mathcal{A})) - \mathbb{P}_{Y_i}(\Phi_i^{-1}(\mathcal{A})) \} \\ &\leq \sup_{\mathcal{A} \subseteq \mathbb{R}^d} \{ \mathbb{P}_{X_{i+1}}(\mathcal{A}) - \mathbb{P}_{\Phi_i(X_i)}(\mathcal{A}) \} + \text{TV}(p_{X_i}, p_{Y_i}) \\ &= \text{TV}(p_{X_{i+1}}, p_{\Phi_i(X_i)}) + \text{TV}(p_{X_i}, p_{Y_i}) \end{aligned} \quad (25)$$

where the first identity arises from the basic property of the TV distance.

Step 2: Simplifying $\text{TV}(p_{X_{i+1}}, p_{\Phi_i(X_i)})$. Next, we recall that $v_i(x) = \frac{x}{t_i} + \frac{1-t_i}{t_i} s_i(x)$. Therefore, by (Liu, 2024, Lemma 13) we have

$$\frac{\partial v_i(x)}{\partial x} = -\frac{1}{1-t_i} I + \frac{t_i}{(1-t_i)^3} \text{Cov}_{1|t_i}(x_i) \quad (26)$$

Further, for any vector $v \in \mathbb{R}^d$ with $\|v\|_2 = 1$ Assumption 4.4(a) tells us that for $i \leq N - 2$

$$\begin{aligned} v^\top \frac{\partial \Phi_i(x)}{\partial x} v &= v^\top \left(I + \eta_i \frac{\partial \hat{v}_i(x)}{\partial x} \right) v = v^\top \left(I + \eta_i \frac{\partial v_i(x)}{\partial x} \right) v + \eta_i v^\top \varepsilon_i^J(x) v \\ &\geq v^\top \left(I + \eta_i \frac{\partial v_i(x)}{\partial x} \right) v - \frac{1}{8} \|v\|_2^2 = v^\top \left\{ \left(1 - \frac{\eta_i}{1-t_i} \right) I + \frac{\eta_i t_i}{(1-t_i)^3} \text{Cov}_{1|t_i}(x) \right\} v - \frac{1}{8} \|v\|_2^2 \\ &\geq \left(1 - h - \frac{1}{8} \right) \|v\|_2^2 > \frac{3}{8}, \quad \text{if } h < 1/2. \end{aligned}$$

Here, the penultimate relation follows from the positive semi-definiteness of the covariance matrix $\text{Cov}_{1|t}(x)$.

Invertibility of $\Phi_i(\cdot)$: The above inequality implies that $\frac{\partial \Phi_i(x)}{\partial x}$ is positive definite uniformly over all x . This entails that $\Phi_i(\cdot)$ is *proper*, i.e., $\lim_{\|x\|_2 \rightarrow \infty} \|\Phi_i(x)\|_2 = \infty$. To see this, we define $\phi(t) := u^\top \Phi_i(tu)$ for a fixed *unit vector* u . Then, we have $\phi'(t) = u^\top \nabla \Phi_i(tu) u > 3/8$. This shows that

$$\phi(t) - \phi(0) = \int_0^t \phi'(u) du \geq 3t/8.$$

An application Cauchy-Schwarz inequality yields

$$\|\Phi_i(tu)\|_2 \geq u^\top \Phi_i(tu) \geq 3t/8 + u^\top \Phi_i(0) \geq 3t/8 - \|\Phi_i(0)\|_2.$$

Setting $t = \|x\|_2$ and $u = x/\|x\|_2$, we have $\|\Phi_i(x)\|_2 \geq 3\|x\|_2/8 - \|\Phi_i(0)\|_2$. This implies that $\Phi_i(\cdot)$ is proper. Then, by Theorem 2.2 of (Ruzhansky & Sugimoto, 2015) shows that $\Phi_i(\cdot)$ is a diffeomorphism. Therefore, we can find a unique x_i such that $\Phi_i(x_i) = x_{i+1}$, which in turn allows us to derive

$$p_{\Phi_i(X_i)}(x_{i+1}) = p_{X_i}(\Phi_i^{-1}(x_i)) \cdot \det\left(\frac{\partial\Phi_i^{-1}(x_{i+1})}{\partial x_{i+1}}\right) = p_{X_i}(x_i) \cdot \det\left(\frac{\partial x_i}{\partial x_{i+1}}\right)$$

Consequently, we see that: for any $i \geq 1$,

$$\begin{aligned} p_{\Phi_i(X_i)}(x_{i+1}) - p_{X_{i+1}}(x_{i+1}) &= p_{X_i}(x_i) \det\left(\frac{\partial x_i}{\partial x_{i+1}}\right) - p_{X_{i+1}}(x_{i+1}) \\ &= \int \left\{ p_{X_t|X_N}(x_i | x_N) \det\left(\frac{\partial x_i}{\partial x_{i+1}}\right) - p_{X_{i+1}|X_N}(x_{i+1} | x_N) \right\} p_{X_N}(x_N) dx_N \\ &= \int \left\{ 1 - \underbrace{\frac{p_{X_{i+1}|X_N}(x_{i+1} | x_N)}{p_{X_i|X_N}(x_i | x_N)} \det\left(\frac{\partial x_{i+1}}{\partial x_i}\right)}_{=: \mathcal{T}(x_i, x_N)} \right\} p_{X_i, X_N}(x_i, x_N) \det\left(\frac{\partial x_i}{\partial x_{i+1}}\right) dx_N \quad (27) \\ &= \int \{1 - \mathcal{T}(x_i, x_N)\} p_{X_i, X_N}(x_i, x_N) \det\left(\frac{\partial x_i}{\partial x_{i+1}}\right) dx_N \end{aligned}$$

Step 3: Analysis of $\mathcal{T}(x_i, x_N)$. The next step is then to analyze $\mathcal{T}(x_i, x_N)$. Controlling $\mathcal{T}(x_i, x_N)$: Given how X_{i+1} and X_i are generated, we observe that

$$\begin{aligned} \mathcal{T}(x_{i+1}, x_N) &= \frac{p_{X_{i+1}|X_N}(x_{i+1} | x_N)}{p_{X_i|X_N}(x_i | x_N)} \det\left(\frac{\partial x_{i+1}}{\partial x_i}\right) = \frac{\left(\frac{1}{1-t_{i+1}}\right)^d \exp\left\{\frac{-\|x_{i+1} - t_{i+1}x_N\|_2^2}{2(1-t_{i+1})^2}\right\}}{\left(\frac{1}{1-t_i}\right)^d \exp\left\{\frac{-\|x_i - t_i x_N\|_2^2}{2(1-t_i)^2}\right\}} \det\left(\frac{\partial x_{i+1}}{\partial x_i}\right) \\ &= \underbrace{\left(\frac{1-t_i}{1-t_{i+1}}\right)^d \det\left(\frac{\partial x_{i+1}}{\partial x_i}\right)}_{=: \mathcal{T}_1(x_i, x_N)} \underbrace{\exp\left\{\frac{\|x_i - t_i x_N\|_2^2}{2(1-t_i)^2} - \frac{\|x_{i+1} - t_{i+1} x_N\|_2^2}{2(1-t_{i+1})^2}\right\}}_{=: \mathcal{T}_2(x_t, x_0)} \end{aligned}$$

leaving us with two terms to control. Let us first study the term $\mathcal{T}_1(x_t, x_0)$, towards which we see that

$$\begin{aligned} \mathcal{T}_1(x_t, x_0) &= \left(\frac{1-t_i}{1-t_{i+1}}\right)^d \det\left(\frac{\partial(x_i + \eta_i \hat{v}_i(x_i))}{\partial x_i}\right) \\ &= \left(\frac{1-t_i}{1-t_{i+1}}\right)^d \det\left(I + \eta_t \frac{\partial}{\partial x_t} v_i(x_i) + \eta_i \left(\frac{\partial}{\partial x_i} \hat{v}_i(x_i) - \frac{\partial}{\partial x_i} v_i(x_i)\right)\right) \\ &\stackrel{(a)}{=} \left(\frac{1-t_i}{1-t_{i+1}}\right)^d \det\left(\left(1 - \frac{\eta_i}{1-t_i}\right) I + \frac{\eta_i t_i}{(1-t_i)^3} \text{Cov}_{1|t_i}(x) + \eta_t \varepsilon_i^J(x_t)\right) \\ &= \det\left(\frac{1-t_i - \eta_i}{1-t_{i+1}} I + \frac{\eta_i t_i}{(1-t_{i+1})(1-t_i)^2} \text{Cov}_{1|t_i}(x_i) + \frac{\eta_i(1-t_i)}{(1-t_{i+1})} \varepsilon_i^J(x_t)\right) \\ &\stackrel{(b)}{=} \det\left(I + \frac{\eta_i t_i}{(1-t_{i+1})(1-t_i)^2} \text{Cov}_{1|t_i}(x_i) + \frac{\eta_i(1-t_i)}{(1-t_{i+1})} \varepsilon_i^J(x_i)\right). \end{aligned}$$

Here, (a) arises from Tweedie's formula, whereas (b) follows since

$$\frac{1-t_i - \eta_i}{1-t_{i+1}} = \frac{1-t_{i+1}}{1-t_{i+1}} = 1.$$

Next, we turn attention to the term $\mathcal{T}_2(x_t, x_0)$, which satisfies

$$\begin{aligned}\log \mathcal{T}_2(x_i, x_N) &= \frac{\|x_i - t_i x_N\|_2^2}{2(1-t_i)^2} - \frac{\|x_{i+1} - t_{i+1} x_N\|_2^2}{2(1-t_{i+1})^2} \\ &= \frac{\|x_i - t_i x_N\|_2^2}{2(1-t_i)^2} - \frac{\|x_i + \eta_i \hat{v}_i(x_i) - t_{i+1} x_N\|_2^2}{2(1-t_{i+1})^2}\end{aligned}\tag{28}$$

We focus on the term $x_i + \eta_i \hat{v}_i(x_i) - t_{i+1} x_N$:

$$\begin{aligned}x_i + \eta_i \hat{v}_i(x_i) - t_{i+1} x_N &= \left(1 - \frac{\eta_i}{1-t_i}\right) x_i + \frac{\eta_i}{1-t_i} \mu_{1|t_i}(x_i) - (t_i + \eta_i) x_N + \eta_i (\hat{v}_i(x_i) - v_i(x_i)) \\ &= \left(1 - \frac{\eta_i}{1-t_i}\right) (x_i - t_i x_N) + \frac{\eta_i}{1-t_i} \mu_{1|t_i}(x_i) - \frac{\eta_i}{1-t_i} t_i x_N - \eta_i x_N + \eta_i (\hat{v}_i(x_i) - v_i(x_i)) \\ &= \left(\frac{1-t_{i+1}}{1-t_i}\right) (x_i - t_i x_N) + \frac{\eta_i}{1-t_i} (\mu_{1|t_i}(x_i) - x_N) + \eta_i \varepsilon_i^v(x_i)\end{aligned}$$

Substitution into (28) yields

$$\begin{aligned}\log \mathcal{T}_2(x_i, x_N) &= -\frac{\eta_i}{(1-t_i)^2(1-t_{i+1})} (x_i - t_i x_N)^\top (\mu_{1|t_i}(x_i) - x_N) - \frac{\eta_i}{(1-t_i)(1-t_{i+1})} (x_i - t_i \mu_{1|t_i}(x_i))^\top \varepsilon_i^v(x_i) \\ &\quad - \frac{\eta_i t_{i+1}}{(1-t_{i+1})^2} (\mu_{1|t_i}(x_i) - x_N) \varepsilon_i^v(x_i) - \frac{\eta_i^2 \|\mu_{1|t_i}(x_i) - x_N\|_2^2}{2(1-t_i)^2(1-t_{i+1})^2} - \frac{\eta_i^2 \|\varepsilon_i^v(x_i)\|_2^2}{2(1-t_{i+1})^2}.\end{aligned}\tag{29}$$

Now Define:

$$\begin{aligned}\xi(x_i, x_N) &:= -\frac{\eta_i (x_i - t_i x_N)^\top (\mu_{1|t_i}(x_i) - x_N)}{(1-t_i)^2(1-t_{i+1})} - \frac{\eta_i t_{i+1} (\mu_{1|t_i}(x_i) - x_N) \varepsilon_i^v(x_i)}{(1-t_{i+1})^2} \\ &\quad - \frac{\eta_i^2 \|\mu_{1|t_i}(x_i) - x_N\|_2^2}{2(1-t_i)^2(1-t_{i+1})^2} + \frac{\eta_i}{(1-t_i)^2(1-t_{i+1})} \left(t_i + \frac{\eta_i}{2(1-t_{i+1})}\right) \text{Tr}(\text{Cov}_{1|t_i})\end{aligned}$$

It is easy to see that

$$\int \xi(x_i, x_N) p_{X_N|X_i=x_i}(x_N) dx_N = 0.$$

Thus, based on (29), we can further simplify $\log \mathcal{T}_2(x_i, x_N)$ as follows:

$$\begin{aligned}\log \mathcal{T}_2(x_i, x_N) &= \xi(x_i, x_N) - \frac{\eta_i (x_i - t_i \mu_{1|t_i}(x_i))^\top \varepsilon_i^v(x_i)}{(1-t_i)(1-t_{i+1})} - \frac{\eta_i^2 \|\varepsilon_i^v(x_i)\|_2^2}{2(1-t_{i+1})^2} \\ &\quad - \frac{\eta_i}{(1-t_i)^2(1-t_{i+1})} \left(t_i + \frac{\eta_i}{2(1-t_{i+1})}\right) \text{Tr}(\text{Cov}_{1|t_i})\end{aligned}$$

Now, for ease of presentation, define

$$\begin{aligned}W(x_i) &:= \log \det \left(I + \frac{\eta_i t_i}{(1-t_{i+1})(1-t_i)^2} \text{Cov}_{1|t_i}(x_i) + \frac{\eta_i (1-t_i)}{(1-t_{i+1})} \varepsilon_i^J(x_i) \right) - \frac{\eta_i^2 \|\varepsilon_i^v(x_i)\|_2^2}{2(1-t_{i+1})^2} \\ &\quad - \frac{\eta_i}{(1-t_i)^2(1-t_{i+1})} \left(t_i + \frac{\eta_i}{2(1-t_{i+1})}\right) \text{Tr}(\text{Cov}_{1|t_i}) - \frac{\eta_i (x_i - t_i \mu_{1|t_i}(x_i))^\top \varepsilon_i^v(x_i)}{(1-t_i)(1-t_{i+1})}\end{aligned}$$

Then for any $x_i \in \mathcal{X}_{\text{data}}$, it holds that

$$\int_{x_N} \left(1 - e^{\xi(x_i, x_N)}\right) e^{W(x_i)} p_{X_N|X_i}(x_N | x_i) dx_N \leq -e^{W(x_i)} \int_{x_N} \xi(x_i, x_N) p_{X_N|X_i}(x_N | x_i) dx_N = 0 \quad (30)$$

where the inequality results from the elementary inequality $1 - e^x \leq -x$ for all $x \in \mathbb{R}$. Using the above quantities and (27) we get: for any $\mathcal{A} \subseteq \mathcal{X}_{\text{data}} \cap \mathcal{E}_i$,

$$\begin{aligned} & \mathbb{P}_{\tilde{\Phi}_i(X_i)}(\mathcal{A}) - \mathbb{P}_{X_{i+1}}(\mathcal{A}) \\ &= \int_{\mathcal{A}} \{1 - \mathcal{T}(x_i, x_N)\} p_{X_i, X_N}(x_i, x_N) \det\left(\frac{\partial x_i}{\partial x_{i+1}}\right) dx_N dx_{i+1} \\ &= \int_{\mathcal{A} \times \mathcal{X}_{\text{data}}} \{1 - \mathcal{T}(x_i, x_N)\} p_{X_N|X_i=x_i}(x_N) p_{X_i}(x_i) \det\left(\frac{\partial x_i}{\partial x_{i+1}}\right) dx_N dx_{i+1} \\ &= \int_{\tilde{\Phi}_i^{-1}(\mathcal{A}) \times \mathcal{X}_{\text{data}}} \{1 - \mathcal{T}(x_i, x_N)\} p_{X_N|X_i=x_i}(x_N) p_{X_i}(x_i) dx_N dx_i \\ &= \int_{\tilde{\Phi}_i^{-1}(\mathcal{A}) \times \mathcal{X}_{\text{data}}} \left\{1 - e^{\xi(x_i, x_N)} \cdot e^{W(x_i)}\right\} p_{X_N|X_i=x_i}(x_N) p_{X_i}(x_i) dx_N dx_i \\ &= \int_{\tilde{\Phi}_i^{-1}(\mathcal{A}) \times \mathcal{X}_{\text{data}}} \left\{\left(1 - e^{\xi(x_i, x_N)}\right) e^{W(x_i)} + \left(1 - e^{W(x_i)}\right)\right\} p_{X_N|X_i=x_i}(x_N) p_{X_i}(x_i) dx_N dx_i \\ &\stackrel{(a)}{\leq} \int_{x_i, x_N \in \tilde{\Phi}_i^{-1}(\mathcal{A}) \times \mathcal{X}_{\text{data}}} \left\{1 - e^{W(x_i)}\right\} p_{X_i, X_N}(x_i, x_N) dx_i dx_N \\ &\leq \int_{x_i \in \tilde{\Phi}_i^{-1}(\mathcal{A})} -W(x_i) p_{X_i}(x_i) dx_i, \end{aligned}$$

where, (a) invokes (30), and the last inequality follows from the elementary inequality $1 - e^x \leq -x$.

Step 4: Analyzing $W(x_i)$. First, we introduce the following lemma from (Liang et al., 2025).

Lemma B.1 (Lemma 5, (Liang et al., 2025)). *Let $A \in \mathbb{R}^{d \times d}$ be a positive-definite matrix, and $\Delta \in \mathbb{R}^{d \times d}$ be any square matrix. Suppose $\eta \|\Delta\|_2 \leq 1/4$, where $\eta \in (0, 1)$. Then it holds that*

$$\log \det(I + \eta A + \eta \Delta) \geq \eta(\text{Tr}(A) + \text{Tr}(\Delta)) - 4\eta^2(\|A\|_F^2 + \|\Delta\|_F^2).$$

Using the above lemma we have

$$\begin{aligned} & -\log \det\left(I + \frac{\eta_i t_i}{(1 - t_{i+1})(1 - t_i)^2} \text{Cov}_{1|t_i}(x_i) + \frac{\eta_i(1 - t_i)}{(1 - t_{i+1})} \varepsilon_i^J(x_i)\right) \\ & \leq \frac{4\eta_i^2 t_i^2}{(1 - t_{i+1})^2(1 - t_i)^4} \|\text{Cov}_{1|t_i}\|_F^2 + \frac{4\eta_i^2(1 - t_i)^2}{(1 - t_{i+1})^2} \|\varepsilon_i^J(x_i)\|_F^2 \\ & \quad - \frac{\eta_i t_i}{(1 - t_{i+1})(1 - t_i)^2} \text{Tr}(\text{Cov}_{1|t_i}) - \frac{\eta_i(1 - t_i)}{(1 - t_{i+1})} \text{Tr}(\varepsilon_i^J(x_i)), \end{aligned}$$

provided that the inequality

$$\frac{\eta_i(1 - t_i)}{(1 - t_{i+1})} \|\varepsilon_i^J(x_i)\|_2 \leq \frac{1}{4}$$

holds for all i . This is indeed the case in our setting, due to Assumption 4.4(a), and

$$\frac{1 - t_i}{1 - t_{i+1}} = \frac{1}{1 - \frac{\eta_i}{1 - t_i}} \leq 2$$

due to the inequality $\frac{\eta_i}{1-t_i} \leq 2h \leq 1/2$, where h is defined in (15). This yields

$$\begin{aligned}
-W(x_i) &= -\log \det \left(I + \frac{\eta_i t_i}{(1-t_{i+1})(1-t_i)^2} \text{Cov}_{1|t_i}(x_i) + \frac{\eta_i(1-t_i)}{(1-t_{i+1})} \varepsilon_i^J(x_i) \right) + \frac{\eta_i^2 \|\varepsilon_i^v(x_i)\|_2^2}{2(1-t_{i+1})^2} \\
&\quad + \frac{\eta_i}{(1-t_i)^2(1-t_{i+1})} \left(t_i + \frac{\eta_i}{2(1-t_{i+1})} \right) \text{Tr}(\text{Cov}_{1|t_i}) + \frac{\eta_i(x_i - t_i \mu_{1|t_i}(x_i))^\top \varepsilon_i^v(x_i)}{(1-t_i)(1-t_{i+1})} \\
&\leq \frac{4\eta_i^2 t_i^2}{(1-t_{i+1})^2(1-t_i)^4} \|\text{Cov}_{1|t_i}(x_i)\|_F^2 + \frac{4\eta_i^2(1-t_i)^2}{(1-t_{i+1})^2} \|\varepsilon_i^J(x_i)\|_F^2 + \frac{\eta_i^2 \|\varepsilon_i^v(x_i)\|_2^2}{2(1-t_{i+1})^2} \\
&\quad + \frac{\eta_i(x_i - t_i \mu_{1|t_i}(x_i))^\top \varepsilon_i^v(x_i)}{(1-t_i)(1-t_{i+1})} + \frac{\eta_i}{(1-t_i)^2(1-t_{i+1})} \left(t_i + \frac{\eta_i}{2(1-t_{i+1})} - t_i \right) \text{Tr}(\text{Cov}_{1|t_i}(x_i)) \\
&\quad - \frac{\eta_i^2(1-t_i)}{(1-t_{i+1})} \text{Tr}(\varepsilon_i^J(x_i)) \\
&\leq \frac{4\eta_i^2 t_i^2}{(1-t_{i+1})^2(1-t_i)^4} \|\text{Cov}_{1|t_i}(x_i)\|_F^2 + \frac{4\eta_i^2(1-t_i)^2}{(1-t_{i+1})^2} \|\varepsilon_i^J(x_i)\|_F^2 + \frac{\eta_i^2 \|\varepsilon_i^v(x_i)\|_2^2}{2(1-t_{i+1})^2} \\
&\quad + \frac{\eta_i^2}{2(1-t_i)^2(1-t_{i+1})^2} \text{Tr}(\text{Cov}_{1|t_i}(x_i)) + \underbrace{\frac{\eta_i(x_i - t_i \mu_{1|t_i}(x_i))^\top \varepsilon_i^v(x_i)}{(1-t_i)(1-t_{i+1})}}_{\Delta(\varepsilon_i^v(x_i))} \\
&\quad - \frac{\eta_i^2(1-t_i)}{(1-t_{i+1})} \text{Tr}(\varepsilon_i^J(x_i)) \\
&\leq \frac{4\eta_i^2 t_i^2}{(1-t_{i+1})^2(1-t_i)^4} \|\text{Cov}_{1|t_i}(x_i)\|_F^2 + \frac{4\eta_i^2(1-t_i)^2}{(1-t_{i+1})^2} \|\varepsilon_i^J(x_i)\|_F^2 + \frac{\eta_i^2 \|\varepsilon_i^v(x_i)\|_2^2}{2(1-t_{i+1})^2} \\
&\quad + \frac{\eta_i^2}{2(1-t_i)^2(1-t_{i+1})^2} \text{Tr}(\text{Cov}_{1|t_i}(x_i)) + \underbrace{\frac{\eta_i(1-t_i)}{(1-t_{i+1})} \frac{(x_i - t_i \mu_{1|t_i}(x_i))^\top \varepsilon_i^v(x_i)}{(1-t_i)^2}}_{\Delta(\varepsilon_i^v(x_i))} \\
&\quad - \frac{\eta_i^2(1-t_i)}{(1-t_{i+1})} \text{Tr}(\varepsilon_i^J(x_i))
\end{aligned} \tag{31}$$

Step 5: Controlling the error arising from $\Delta(\varepsilon_i^v(x_i))$. We start with the following integral quantity for any set \mathcal{A} :

$$\begin{aligned}
&\int_{x_i \in \mathcal{A}} \frac{1}{(1-t_i)^2} (x_i - t_i \mu_{1|t_i}(x_i))^\top \varepsilon_i^v(x_i) p_{X_i}(x_i) \, dx_i \\
&= \int_{x_i, x_N \in \mathcal{A} \times \mathcal{X}_{\text{data}}} \frac{1}{(1-t_i)^2} (x_i - t_i \mu_{1|t_i}(x_i))^\top \varepsilon_i^v(x_i) p_{X_i, X_N}(x_i, x_N) \, dx_i \, dx_N \\
&= \int_{x_i, x_N \in \mathcal{A} \times \mathcal{X}_{\text{data}}} \frac{1}{(1-t_i)^2} (x_i - t_i \mu_{1|t_i}(x_i))^\top \varepsilon_i^v(x_i) p_{X_N|X_i=x_i}(x_N) p_{X_i}(x_i) \, dx_N \, dx_i \\
&= \int_{x_i, x_N \in \mathcal{A} \times \mathcal{X}_{\text{data}}} \frac{1}{(1-t_i)^2} (x_i - t_i \mu_{1|t_i}(x_i))^\top \varepsilon_i^v(x_i) p_{X_i|X_N=x_N}(x_i) p_{X_N}(x_N) \, dx_i \, dx_N \\
&= \int_{x_i, x_N \in \mathbb{R}^d \times \mathcal{X}_{\text{data}}} \frac{1}{(1-t_i)^2} \{ (x_i - t_i x_N)^\top \varepsilon_i^v(x_i) p_{X_i|X_N=x_N}(x_i) \, dx_i \} p_{X_N}(x_N) \, dx_N \\
&\leq \int_{x_i, x_N \in \mathbb{R}^d \times \mathcal{X}_{\text{data}}} \frac{1}{(1-t_i)^2} \{ |(x_i - t_i x_N)^\top \varepsilon_i^v(x_i)| p_{X_i|X_N=x_N}(x_i) \, dx_i \} p_{X_N}(x_N) \, dx_N \\
&\leq \left(\int_{x_i, x_N \in \mathbb{R}^d \times \mathcal{X}_{\text{data}}} \left\{ \frac{1}{(1-t_i)^4} |(x_i - t_i x_N)^\top \varepsilon_i^v(x_i)|^2 p_{X_i|X_N=x_N}(x_i) \, dx_i \right\} p_{X_N}(x_N) \, dx_N \right)^{1/2} \\
&= \left(\int_{x_i, x_N \in \mathbb{R}^d \times \mathcal{X}_{\text{data}}} \left\{ \frac{1}{(1-t_i)^4} \langle (x_i - t_i x_N)(x_i - t_i x_N)^\top, \varepsilon_i^v(x_i) \varepsilon_i^v(x_i)^\top \rangle p_{X_i|X_N=x_N}(x_i) \, dx_i \right\} p_{X_N}(x_N) \, dx_N \right)^{1/2}
\end{aligned} \tag{32}$$

Now, recall that $X_i \mid X_N = x_N \sim N(t_i x_N, (1 - t_i)^2 I)$. Using standard techniques from (Liang et al., 2025, Section B.5), we can obtain bound on (32):

$$\int_{x_i \in \mathcal{A}} \frac{1}{(1 - t_i)^2} (x_i - t_i \mu_{1|t_i}(x_i))^\top \varepsilon_i^v(x_i) p_{X_i}(x_i) dx_i \leq \frac{2\varepsilon_i^v}{(1 - t_i)} + \varepsilon_i^{J,1} + \varepsilon_i^{J,2} + \varepsilon_i^H.$$

Substituting this in (31), we have

$$\begin{aligned} & \int_{x_i \in \mathcal{A}} \left\{ \Delta(\varepsilon_i^v(x_i)) - \frac{\eta_i^2(1 - t_i)}{(1 - t_{i+1})} \text{Tr}(\varepsilon_i^J(x_i)) \right\} p_{X_i}(x_i) \\ & \leq \frac{2\varepsilon_i^v}{(1 - t_i)} + \varepsilon_i^{J,1} + \varepsilon_i^{J,2} + \varepsilon_i^H + \frac{\eta_i^2(1 - t_i)}{(1 - t_{i+1})} \left(\int \text{Tr}(\varepsilon_i^J(x_i))^2 p_{X_i}(x_i) dx_i \right)^{1/2} \\ & \leq \frac{2\eta_i}{(1 - t_{i+1})} (\varepsilon_i^v + \varepsilon_i^{J,1} + \varepsilon_i^{J,2} + \varepsilon_i^H). \end{aligned}$$

Here, we used the fact that $\frac{\eta_i^2(1 - t_i)}{(1 - t_{i+1})} \leq \frac{\eta_i}{(1 - t_{i+1})}$.

Step 6: Bounding the terms involving $\text{Cov}_{1|t_i}(x_i)$. Here we always assume that $k \geq \log d$.¹ We begin defining some quantities first.

- Let $\{x_i^*\}_{1 \leq i \leq N_{\epsilon_0}}$ be an ϵ_0 -net of $\mathcal{X}_{\text{data}}$, with N_{ϵ_0} denoting its cardinality. Let $\{B_i\}_{1 \leq i \leq N_{\epsilon_0}}$ be a disjoint ϵ_0 -cover for $\mathcal{X}_{\text{data}}$ such that $x_i^* \in B_i$ for each i .
- Define the following two sets:

$$\mathcal{I} := \{1 \leq i \leq N_{\epsilon_0} : \mathbb{P}(X_0 \in B_i) \geq \exp(-C_1 k \log T)\} \quad (33)$$

and

$$\mathcal{G} := \left\{ w \in \mathbb{R}^d : \|w\|_2 \leq 2\sqrt{d} + \sqrt{C_1 k \log T}, |(x_i^* - x_j^*)^\top w| \leq \sqrt{C_1 k \log T} \|x_i^* - x_j^*\|_2, \forall 1 \leq i, j \leq N_{\epsilon_0} \right\}. \quad (34)$$

for some sufficiently large universal constant $C_1 > 0$. As it turns out, $\bigcup_{i \in \mathcal{I}} B_i$ and \mathcal{G} form certain high-probability sets related to the random vector $X_0 \sim p_{\text{data}}$ and the standard Gaussian random vector in \mathbb{R}^d , respectively.

- Recall (24), we can express

$$X_{t_i} \equiv X_i = t_i X_N + (1 - t_i) X_0, \quad (35)$$

for some random vector $X_0 \sim \mathcal{N}(0, I_d)$.

Next, we define the set $\mathcal{T}_t := \{tv_1 + (1 - t)\omega : v_1 \in \bigcup_{i \in \mathcal{I}} B_i, \omega \in \mathcal{G}\}$.

Borrowing standard techniques and results from the proofs of (Liang et al., 2025, Lemma 1) and (Liang et al., 2025, Corollary 1), we have the following results

$$\mathbb{P}(X_i \notin \mathcal{T}_{t_i}) \leq \exp(-C_2 k \log N), \quad \text{for } C_2 \gg C_{\text{cover}}, \text{ and } 0 \leq t_i < 1. \quad (36)$$

$$\text{Tr}(\text{Cov}_{1|t_i}(x_i)) \leq \frac{C_3(1 - t_i)^2}{t_i^2} k \log N, \quad \text{for all } t_i > 0 \text{ and } x_i \in \mathcal{T}_{t_i}. \quad (37)$$

Step 7: Bound on the term involving squared Frobenius norm using linearization: One can use (37) directly to bound the term $\mathbb{E}_{X_i} (\|\text{Cov}_{1|t_i}(X_i)\|_F^2)$ in (31). However, this will lead to a quadratic dependence on k . Therefore, we present the following lemma that will yield a linear dependence on k . The proof is deferred to Appendix D.2.

¹If $k < \log d$, then we can redefine k as $\log d$. This does not change the results in Theorem 4.5 and Theorem 4.7.

Proposition B.2. For all $i \geq 1$, the following holds:

$$\frac{\eta_i t_i}{(1-t_{i+1})^2(1-t_i)^2} \mathbb{E}(\|Cov_{1|t_i}(X_i)\|_F^2) \leq \frac{3}{4} (\mathbb{E}[\text{Tr}(Cov_{1|t_i}(X_i))] - \mathbb{E}[\text{Tr}(Cov_{1|t_{i+1}}(X_{i+1}))]) + \frac{6h\eta_i}{(1-t_{i+1})^2 N^{10}}.$$

The

Using Proposition B.2 and (37), we have

$$\begin{aligned} & \mathbb{P}_{\tilde{\Phi}_i(X_i)}(\mathcal{A}) - \mathbb{P}_{X_{i+1}}(\mathcal{A}) \\ &= \mathbb{P}(\tilde{\Phi}_i(X_i) \in \mathcal{A}, X_i \in \mathcal{E}_i) - \mathbb{P}(X_{i+1} \in \mathcal{A}) + \mathbb{P}(X_i \notin \mathcal{E}_i) \\ &\leq \mathbb{P}(\tilde{\Phi}_i(X_i) \in \mathcal{A}, \tilde{\Phi}(X_i) \in \tilde{\Phi}(\mathcal{E}_i)) - \mathbb{P}(X_{i+1} \in \mathcal{A}) + \mathbb{P}(X_i \notin \mathcal{E}_i) \\ &\leq \mathbb{P}(\tilde{\Phi}_i(X_i) \in \mathcal{A} \cap \tilde{\Phi}(\mathcal{E}_i)) - \mathbb{P}(X_{i+1} \in \mathcal{A} \cap \tilde{\Phi}(\mathcal{E}_i)) + \mathbb{P}(X_i \notin \mathcal{E}_i) \\ &\leq \frac{3\eta_i t_i}{(1-t_i)^2} \left(\frac{(1-t_i)^2}{t_i^2} - \frac{(1-t_{i+1})^2}{t_{i+1}^2} \right) k \log N + \frac{\eta_i^2}{2(1-t_{i+1})^2 t_i^2} k \log N + \frac{4\eta_i^2(1-t_i)^2}{(1-t_{i+1})^2} (\varepsilon_i^{J,1})^2 + \frac{\eta_i^2}{2(1-t_i)^2} (\varepsilon_i^V)^2 \\ &\quad + \frac{2\eta_i}{(1-t_{i+1})} (\varepsilon_i^V + \varepsilon_i^{J,1} + \varepsilon_i^{J,2} + \varepsilon_i^H) + \mathbb{P}(X_i \notin \mathcal{E}_i) + \frac{24h\eta_i^2 t_i}{(1-t_{i+1})^2(1-t_i)^2 N^{10}}. \end{aligned}$$

First, Lemma D.2 yields that

$$\frac{(1-t_i)^2}{t_i^2} - \frac{(1-t_{i+1})^2}{t_{i+1}^2} \leq \frac{2\eta_i}{t_i^3}. \quad (38)$$

We also use the Markov's inequality to control the following:

$$\mathbb{P}(X_i \notin \mathcal{E}_i) = \mathbb{P} \left\{ \frac{\eta_i(1-t_i)}{(1-t_{i+1})} \|\varepsilon_i^J(x_i)\| > \frac{1}{8} \right\} \leq \frac{64\eta_i^2(1-t_i)^2}{(1-t_{i+1})^2} \mathbb{E} \{ \|\varepsilon_i^J(x_i)\|^2 \} \leq \frac{64\eta_i^2(1-t_i)^2}{(1-t_{i+1})^2} (\varepsilon_i^{J,1})^2.$$

Using the above inequality along with (38) yields

$$\begin{aligned} & \mathbb{P}_{\tilde{\Phi}_i(X_i)}(\mathcal{A}) - \mathbb{P}_{X_{i+1}}(\mathcal{A}) \\ &\leq \frac{6C_3\eta_i^2}{(1-t_{i+1})^2 t_i^2} k \log N + \frac{C_3\eta_i^2}{2(1-t_{i+1})^2 t_i^2} k \log N + \frac{C\eta_i^2(1-t_i)^2}{(1-t_{i+1})^2} (\varepsilon_i^{J,1})^2 + \frac{\eta_i^2}{2(1-t_i)^2} (\varepsilon_i^V)^2 \\ &\quad + \frac{2\eta_i}{(1-t_{i+1})} (\varepsilon_i^V + \varepsilon_i^{J,1} + \varepsilon_i^{J,2} + \varepsilon_i^H) + \frac{24h\eta_i^2 t_i}{(1-t_{i+1})^2(1-t_i)^2 N^{10}}. \end{aligned}$$

Few properties of time scheduling (15):

1. For all $i > 1$, we have $\frac{\eta_i}{1-t_i} \leq 2h$ and $\frac{\eta_i}{1-t_{i+1}} \leq 2h$.
2. For all $i > 1$, we have $\frac{\eta_i^2(1-t_i)^2}{(1-t_{i+1})^2} = \frac{(1-t_i)^2}{(\frac{1-t_i}{\eta_i}-1)^2} \leq 4h^2$, as $\frac{\eta_i}{(1-t_i)} \leq 2h$ and $(1-t_i) \leq 1$.
3. $\sum_{i:t_i>0} \frac{\eta_i^2}{(1-t_{i+1})^2 t_i^2} = \sum_{i:0 < t_{i+1} \leq 1/2} \frac{\eta_i^2}{(1-t_{i+1})^2 t_i^2} + \sum_{i:t_{i+1}>1/2} \frac{\eta_i^2}{(1-t_{i+1})^2 t_i^2} \leq 4h^2 N$.

Putting all of these together and solving (25), we get

$$\begin{aligned} & \text{TV}(p_{X_{N-1}}, p_{Y_{N-1}}) \\ &\leq C'_1 h^2 N k \log N + C'_2 h^2 N \varepsilon_{J,1}^2 + C'_3 h^2 N \varepsilon_v^2 \\ &\quad + C'_4 h \times \sum_{i=1}^{N-1} (\varepsilon_i^V + \varepsilon_i^{J,1} + \varepsilon_i^{J,2} + \varepsilon_i^H) + C'_5 \frac{h^2}{\delta^2 N^{10}} + \text{TV}(p_{X_1}, p_{Y_1}) \\ &\leq C'_1 h^2 N k \log N + C'_2 h^2 N \varepsilon_{J,1}^2 + C'_3 h^2 N \varepsilon_v^2 \\ &\quad + C'_4 h N (\varepsilon_v + \varepsilon_{J,1} + \varepsilon_{J,2} + \varepsilon_H) + C'_5 \frac{h^2}{\delta^2 N^{10}} + \text{TV}(p_{X_1}, p_{Y_1}), \end{aligned}$$

for sufficiently large N .

Handling $\text{TV}(p_{X_1}, p_{Y_1})$ separately: Recall that (31) is also valid for $t_{i+1} = \delta, t_i = 0$. Therefore, we have

$$\begin{aligned} & -W(x_0) \\ & \leq \frac{4\delta^2}{(1-\delta)^2} \|\varepsilon_0^J(x_0)\|_F^2 + \frac{\delta^2 \|\varepsilon_0^V(x_0)\|_2^2}{2(1-\delta)^2} + \frac{\delta^2}{2(1-\delta)^2} \text{Trace}(\text{Cov}_1) + \underbrace{\frac{\delta}{1-\delta} x_0^\top \varepsilon_0^V(x_0)}_{\Delta(\varepsilon_0^V(x_0))} \\ & \quad - \frac{\delta^2}{(1-\delta)} \text{Trace}(\varepsilon_0^J(x_0)). \end{aligned}$$

Therefore, applying similar argument, we get

$$\text{TV}(p_{X_1}, p_{Y_1}) \leq A_1 \delta^2 \text{Trace}(\text{Cov}_1) + A_2 \delta^2 (\varepsilon_0^V)^2 + A_3 \delta^2 (\varepsilon_0^{J,1})^2 + A_4 (\varepsilon_0^V + \varepsilon_0^{J,1} + \varepsilon_0^{J,2} + \varepsilon_0^H) + \underbrace{\text{TV}(p_{X_0}, p_{Y_0})}_{=0}.$$

Now we recall that $\delta < 1/N$. Therefore, combining all of the above inequalities and (16) gives

$$\begin{aligned} & \text{TV}(p_{X_{N-1}}, p_{Y_{N-1}}) \\ & \leq C_1'' \frac{k \log^3(1/\delta)}{N} + C_2'' \frac{\log^2(1/\delta)}{N} \varepsilon_{J,1}^2 + C_3'' \frac{\log^2(1/\delta)}{N} \varepsilon_V^2 \\ & \quad + C_4'' \log(1/\delta) (\varepsilon_V + \varepsilon_{J,1} + \varepsilon_{J,2} + \varepsilon_H) + C_5'' \delta^{-2} N^{-10} \\ & \quad + A_1 \delta^2 \text{Trace}(\text{Cov}_1) + A_2 \delta^2 (\varepsilon_0^V)^2 + A_3 \delta^2 (\varepsilon_0^{J,1})^2 + A_4 (\varepsilon_0^V + \varepsilon_0^{J,1} + \varepsilon_0^{J,2} + \varepsilon_0^H). \end{aligned}$$

Now, note that one can estimate $v_0(x) = \mu_{p_{X_1}} - x$ by $\hat{v}_0(x) := \hat{\mu}_1 - x$, where $\hat{\mu}_1 = \sum_{i=1}^n x_{i,1}/n$ and n is the (training) sample size. In this case, we have

- $\varepsilon_0^{J,1} = \varepsilon_0^{J,2} = \varepsilon^H = 0$.
- $(\varepsilon_0^V)^2 = \mathbb{E} \|\hat{\mu}_1 - \mu_{p_{X_1}}\|_2^2 = O\left(\frac{\text{Trace}(\text{Cov}_1)}{n}\right)$.

This finishes the proof of Theorem 4.5.

B.3. Proof of convergence of Stoc-RF (Theorem 4.7)

The proof of this result essentially follows by reduction and leverages key results of (Liang et al., 2025). We start by recalling some key facts: $t(\tau) = \frac{\sqrt{\omega_\tau}}{\sqrt{1-\omega_\tau} + \sqrt{\omega_\tau}}$, and $\frac{Y'_\tau}{\sqrt{\omega_\tau}} \stackrel{d}{=} \frac{\tilde{Z}_{t(\tau)}}{t(\tau)}$. With this time transformation, we have

$$\alpha_\tau = \frac{\omega_\tau}{\omega_{\tau-1}} = \frac{(t_i/\sigma_{t_i})^2}{(t_{i+1}/\sigma_{t_{i+1}})^2} = \frac{R_i^2}{R_{i+1}^2}, \quad \text{where } t_i = t(\tau). \quad (39)$$

We also have $s_{Y'_\tau}(y) = \sigma_t s_{\tilde{Z}_t}(\tilde{z})$, where $\tilde{z} = \sigma_t y$. Next, we recall the DDIM sampler considered in (Liang et al., 2025):

$$\begin{aligned} \hat{Y}'_{\tau-1} &= \frac{1}{\sqrt{\alpha_\tau}} \left\{ \hat{Y}'_\tau + \delta_\tau \hat{s}_{Y'_\tau}(\hat{Y}'_\tau) + \nu_\tau \xi_\tau \right\}, \hat{Y}'_N \sim N(0, I_d) \\ \delta_\tau &= 1 - \alpha_\tau, \nu_\tau = \sqrt{\frac{(\alpha_\tau - \omega_\tau)(1 - \alpha_t)}{1 - \omega_\tau}}, \\ \tau &= N, N-1, \dots, 1, \quad \{\xi_\tau\}_{\tau \geq 1} \stackrel{i.i.d.}{\sim} N(0, I_d), \end{aligned} \quad (40)$$

Now, if we substitute all the quantities of the above sampler by its corresponding RF eversions, i.e., we get $\hat{Y}_\tau \rightarrow$

$Y_t/\sigma_t, \hat{s}_{Y'_\tau}(y) \rightarrow \sigma_t \hat{s}_{t_i}(Y_{t_i})$, and $\alpha_\tau \rightarrow \frac{R_i^2}{R_{i+1}^2}$, then it leads to the following sampler:

$$\begin{aligned} \frac{Y_{t_{i+1}}}{\sigma_{t_{i+1}}} &= \frac{R_{i+1}}{R_i} \left\{ \frac{Y_{t_i}}{\sigma_{t_i}} + \eta_i \sigma_{t_i} \hat{s}_{t_i}(Y_{t_i}) + \sqrt{\psi_i} W_{t_i} \right\}, \\ \frac{Y_{t_0}}{\sigma_{t_0}} &\sim N(0, I_d), \quad \{W_{t_i}\}_{i \geq 0} \stackrel{i.i.d.}{\sim} N(0, I_d), \\ i &= 0, 1, \dots, N-1, \end{aligned} \tag{41}$$

where $\eta_i = 1 - \frac{R_i^2}{R_{i+1}^2}$, $\psi_i = \frac{R_i^2}{R_{i+1}^2} \cdot \frac{1-R_{i+1}^2}{1-R_i^2} \cdot \left(1 - \frac{R_i^2}{R_{i+1}^2}\right)$, and $\hat{s}_{t_i}(x) = \frac{t_i \hat{v}_{t_i}(x) - x}{1-t_i}$. The above is exactly the sampler described in (21). In other words, we have equivalence between two above samplers. Therefore, we can use the convergence result of (40).

Defining few auxiliary processes: We define the auxiliary processes in exact way defined in (Liang et al., 2025, Section C.1).

- First, we define $\{Y_\tau^*\}_{\tau=N}^1$ by

$$Y_N^* = Y'_N \sim N(0, I_d), \quad Y_{\tau-1}^* = \frac{1}{\sqrt{\alpha_\tau}} (Y_\tau^* + \delta_\tau s_{Y'_\tau}(Y_\tau^*) + \nu_\tau \xi_\tau).$$

- We construct an auxiliary process \bar{Y}_τ that follows the same transition dynamics as Y_τ^* :

$$\bar{Y}_{\tau-1}^- \mid \bar{Y}_\tau \sim Y_{\tau-1}^* \mid Y_\tau^*, \quad \bar{Y}_{\tau-1}^- \left| \left\{ \bar{Y}_{\tau-1}^- = y_{\tau-1}^- \right\} \right. = \begin{cases} y_{\tau-1}^-, & \text{with prob. } \frac{p_{Y'_\tau}(y_{\tau-1}^-)}{p_{\bar{Y}_{\tau-1}^-}(y_{\tau-1}^-)} \wedge 1 \\ \infty, & \text{otherwise} \end{cases} \tag{42}$$

for any $y_{\tau-1}^- \neq \infty$, where we recall that $a \wedge b := \min\{a, b\}$. It is straightforward to show that

$$p_{\bar{Y}_\tau}(y_\tau) = \int_{\mathbb{R}^d} (p_{Y'_\tau}(y_\tau^-) \wedge p_{\bar{Y}_\tau^-}(y_\tau^-)) \delta(y_\tau - y_\tau^-) dy_\tau^- = p_{Y'_\tau}(y_\tau) \wedge p_{\bar{Y}_\tau^-}(y_\tau) \tag{43}$$

for any $y_\tau \neq \infty$, where $\delta(\cdot)$ denotes the Dirac measure.

- To account for the score estimation error, we introduce another auxiliary process \tilde{Y}_τ based on the dynamics of Y_τ :

$$\tilde{Y}_{\tau-1}^- \mid \tilde{Y}_\tau \sim \hat{Y}'_{\tau-1} \mid \hat{Y}_\tau', \quad \tilde{Y}_{\tau-1}^- \left| \left\{ \tilde{Y}_{\tau-1}^- = y_{\tau-1}^- \right\} \right. = \begin{cases} y_{\tau-1}^-, & \text{with prob. } \frac{p_{Y'_\tau}(y_{\tau-1}^-)}{p_{\tilde{Y}_{\tau-1}^-}(y_{\tau-1}^-)} \wedge 1 \\ \infty, & \text{otherwise.} \end{cases} \tag{44}$$

Next, we observe that for $t_i = t(\tau)$

$$(\varepsilon_\tau^s)^2 := \mathbb{E} \|\hat{s}_{Y'_\tau}(Y'_\tau) - s_{Y'_\tau}(Y'_\tau)\|_2^2 = \sigma_{t_i}^2 \mathbb{E} \|\hat{s}_{t_i}(X_{t_i}) - s_{t_i}(X_{t_i})\|_2^2 \leq (\varepsilon_s^s)^2. \tag{45}$$

Now, we can exactly replicate the analysis in Liang et al. (2025, Section C.2) till Equation (107) in Step 6, which yields the following for a universal constant $L > 0$:

$$\text{KL} \left(p_{\bar{Y}_1} \| p_{\tilde{Y}_1} \right) \leq \sum_{\tau=2}^N L(1 - \omega_\tau) (\varepsilon_\tau^s)^2 \lesssim \frac{\log N}{N} \sum_{t_i=t(2)}^{t(N)} (\varepsilon_i^s)^2 \lesssim \varepsilon_s^2 \log N.$$

After this, Step 7 of the proof follows verbatim to yield the final bound in Theorem 4.7.

B.4. Description of the new RF sampler in Remark 4.8

The DDIM sampler considered in Liang et al. (2025) is the following:

$$\begin{aligned}\hat{Y}'_{\tau-1} &= \frac{1}{\sqrt{\alpha_\tau}} \left\{ \hat{Y}'_\tau + \delta_\tau \hat{s}_{Y'_\tau}(\hat{Y}'_\tau) \right\}, \quad \hat{Y}'_N \sim N(0, I_d) \\ \delta_\tau &= \frac{1 - \alpha_\tau}{1 + \sqrt{\frac{\alpha_\tau - \omega_\tau}{1 - \omega_\tau}}}, \\ \tau &= N, N-1, \dots, 1.\end{aligned}\tag{46}$$

Next, using the same set of transformations as in Section B.3 and plugging it in (46), we arrive at the following RF sampler:

$$\begin{aligned}\frac{Y_{t_{i+1}}}{\sigma_{t_{i+1}}} &= \frac{R_{i+1}}{R_i} \left\{ \frac{Y_{t_i}}{\sigma_{t_i}} + \eta_i \sigma_{t_i} \hat{s}_{t_i}(Y_{t_i}) \right\}, \\ \frac{Y_{t_0}}{\sigma_{t_0}} &\sim N(0, I_d), \\ i &= 0, 1, \dots, N-1,\end{aligned}\tag{47}$$

$$\text{where } \eta_i = \frac{1 - \frac{R_i^2}{R_{i+1}^2}}{1 + \sqrt{\frac{R_i^2}{R_{i+1}^2} \cdot \frac{1 - R_{i+1}^2}{1 - R_i^2}}}, \quad R_i = t_i / \sigma_{t_i}.$$

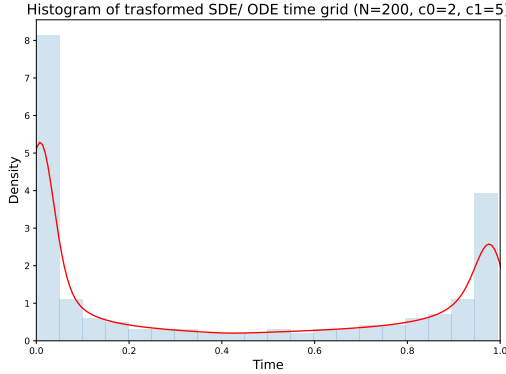


Figure 7. Histogram and KDE plot of the transformed time-grid (18) showing U-shaped distribution.

Algebraic simplification. Using $R_i = t_i / \sigma_{t_i}$, we have

$$\frac{R_{i+1}}{R_i} = \frac{t_{i+1}}{t_i} \frac{\sigma_{t_i}}{\sigma_{t_{i+1}}}, \quad \frac{R_i^2}{R_{i+1}^2} \cdot \frac{1 - R_{i+1}^2}{1 - R_i^2} = \frac{t_i^2 (1 - t_{i+1})^2}{t_{i+1}^2 (1 - t_i)^2}, \quad \eta_i = \frac{1 - \frac{t_i^2 \sigma_{t_{i+1}}^2}{t_{i+1}^2 \sigma_{t_i}^2}}{1 + \frac{t_i (1 - t_{i+1})}{t_{i+1} (1 - t_i)}}.$$

Multiplying (47) by $\sigma_{t_{i+1}}$ yields

$$Y_{t_{i+1}} = \frac{t_{i+1}}{t_i} \left(Y_{t_i} + \eta_i \sigma_{t_i}^2 \hat{s}_{t_i}(Y_{t_i}) \right).$$

A direct calculation using $\sigma_t^2 = t^2 + (1 - t)^2$ shows that

$$\eta_i \sigma_{t_i}^2 = \frac{(t_{i+1} - t_i)(1 - t_i)}{t_{i+1}}.$$

Therefore, the deterministic sampler can be written equivalently as

$$Y_{t_{i+1}} = \frac{t_{i+1}}{t_i} Y_{t_i} + \frac{(t_{i+1} - t_i)(1 - t_i)}{t_i} \hat{s}_{t_i}(Y_{t_i}) = Y_{t_i} + \Delta_i \left\{ \frac{Y_{t_i}}{t_i} + \frac{1 - t_i}{t_i} \hat{s}_{t_i}(Y_{t_i}) \right\},\tag{48}$$

where $\Delta_i = t_{i+1} - t_i$. This expression matches exactly the form of the RF sampler in (5). However, the time steps Δ_i are different from those we propose in (15), which we used to obtain the RF convergence guarantees given in Theorem 4.5. Although the time-schedule is still U-shaped as shown in Figure 7.

C. Proof of Lemmas related to Stochastic Localization (Section 3)

C.1. Proof of Lemma 3.2 and Lemma 3.3

We first show that the solution to the SDE (11) takes the form

$$\frac{Y'_\tau}{\sqrt{\omega_\tau}} = X_1 + \tilde{B}'_{\frac{1-\omega_\tau}{\omega_\tau}}, \quad (49)$$

where $\omega_\tau = \exp(-2 \int_0^\tau \beta(u) du)$ and $\{\tilde{B}'_\tau\}_{\tau \geq 0}$ is a standard Brownian motion. First, it is easy to see that the solution of SDE (11) is

$$\frac{Y'_\tau}{\sqrt{\omega_\tau}} = X_1 + \underbrace{\int_0^\tau \sqrt{2\beta(t)} \exp\left(\int_0^t \beta(u) du\right) dB'_t}_{:= M_\tau}. \quad (50)$$

We note that M_τ is continuous local Martingale with $M_0 = 0$. Also, the quadratic variation of M_τ is

$$\langle M \rangle_\tau = \int_0^\tau 2\beta(t) \exp\left(2 \int_0^t \beta(u) du\right) dt = \exp\left(2 \int_0^\tau \beta(u) du\right) - 1 = \frac{1 - \omega_\tau}{\omega_\tau}.$$

Then, by Dambis–Dubins–Schwarz theorem (Revuz & Yor, 2013, Theorem 1.6) there exists a Brownian motion $\{\tilde{B}'_u\}_{u \geq 0}$ such that $\{M_\tau\}_{\tau \geq 0} = \{\tilde{B}'_{\frac{1-\omega_\tau}{\omega_\tau}}\}_{\tau \geq 0}$. Therefore, we have (49) by substituting M_τ in (50).

Now, we define two processes : $\hat{U}_s := sY'_{\tau(s)}/\sqrt{\omega_{\tau(s)}} = sX_1 + s\tilde{B}'_{\frac{1-\omega_{\tau(s)}}{\omega_{\tau(s)}}}$, and $\tilde{U}_s := s\tilde{X}_{t(s)}/t(s) = sX_1 + s\tilde{B}_{\frac{(1-t(s))^2}{t^2(s)}}$.

Now, under the prescribed time change in Lemma 3.2 and Lemma 3.3, we have

$$s\tilde{B}'_{\frac{1-\omega_{\tau(s)}}{\omega_{\tau(s)}}} = s\tilde{B}'_{1/s}, \quad \text{and} \quad s\tilde{B}_{\frac{(1-t(s))^2}{t^2(s)}} = s\tilde{B}_{1/s}.$$

Note, that both $\{s\tilde{B}'_{1/s}\}_{s \geq 0}$ and $\{s\tilde{B}_{1/s}\}_{s \geq 0}$ are Brownian motions. Hence, $\{\hat{U}_s\}_{s \geq 0}$ and $\{\tilde{U}_s\}_{s \geq 0}$ are equivalent to SL process.

C.2. Proof of Lemma 3.4: Equivalence of SDE (6) and SDE (12)

SDE (6) to SDE (12):

We begin with the SDE of \tilde{Z}_t :

$$d\tilde{Z}_t = \left\{ \frac{\tilde{Z}_t}{t} + 2 \left(\frac{1-t}{t} \right) s_t(\tilde{Z}_t) \right\} dt + \sqrt{2 \left(\frac{1-t}{t} \right)} dB_t, \quad (51)$$

where $s_t(\cdot)$ is the score of \tilde{Z}_t , and $\{B_t\}_{t \geq 0}$ is Brownian motion.

Recall the transformation $t(\tau) = \frac{\sqrt{\omega_\tau}}{\sqrt{\omega_\tau} + \sqrt{1-\omega_\tau}}$, where $\omega(\tau) = \exp(-2 \int_0^\tau \beta(u) du)$.

Now, we define $\hat{Y}_\tau := \frac{\sqrt{\omega_{N-\tau}} \tilde{Z}_{t(N-\tau)}}{t(N-\tau)}$. We first begin by noting that $\frac{\sqrt{\omega_{N-\tau}}}{t(N-\tau)} = \frac{1}{\sigma_{t(N-\tau)}}$. We also have $\log \omega_{N-\tau} =$

$-2 \int_0^{N-\tau} \beta(u) du$. Therefore, we have

$$\begin{aligned} \frac{1}{\omega_{N-\tau}} \cdot \frac{d\omega_{N-\tau}}{dt} &= 2\beta(N-\tau) \frac{d\tau}{dt} \\ \Rightarrow \frac{d\tau}{dt} &= \frac{1}{2\beta(N-\tau)\omega(N-\tau)} \cdot \frac{d\omega_{N-\tau}}{dt} = \frac{1}{2\beta(N-\tau)\omega(N-\tau)} \cdot \frac{d(t^2/\sigma_t^2)}{dt} \\ \Rightarrow \frac{d\tau}{dt} &= \frac{1}{\beta(N-\tau)} \cdot \frac{1-t}{t\sigma_t^2} \end{aligned} \quad (52)$$

Next, we define the backward time $t_\tau := t(N-\tau)$, and then we can write $\tilde{Z}_{t_\tau} = \sigma_{t_\tau} \overleftarrow{Y}_\tau$. This also yields that the score of \overleftarrow{Y}_τ satisfies $s_\tau^\leftarrow(\overleftarrow{Y}_\tau) = \sigma_{t_\tau} s_t(\tilde{Z}_{t_\tau})$. Moreover, (14) yields that $\sigma_{t_\tau} s_t(\tilde{Z}_{t_\tau}) = \nabla \log q_{N-\tau}(\overleftarrow{Y}_\tau)$. Next, with (53) and (51) in mind, we can write

$$\begin{aligned} d\overleftarrow{Y}_\tau &= \frac{1}{\sigma_{t_\tau}} d\tilde{Z}_{t_\tau} - \frac{2t-1}{\sigma_{t_\tau}^3} \tilde{Z}_{t_\tau} dt_\tau \\ &= \left\{ \frac{\tilde{Z}_{t_\tau}}{t_\tau \sigma_{t_\tau}} + 2 \left(\frac{1-t_\tau}{t_\tau \sigma_{t_\tau}} \right) s_{t_\tau}(\tilde{Z}_{t_\tau}) - \frac{2t_\tau-1}{\sigma_{t_\tau}^3} \tilde{Z}_{t_\tau} \right\} dt_\tau + \sqrt{2 \left(\frac{1-t_\tau}{\sigma_{t_\tau}^2 t_\tau} \right)} dB_{t_\tau} \\ &= \left\{ \frac{1-t_\tau}{t_\tau \sigma_{t_\tau}^3} \tilde{Z}_{t_\tau} + 2 \left(\frac{1-t_\tau}{t_\tau \sigma_{t_\tau}} \right) s_{t_\tau}(\tilde{Z}_{t_\tau}) \right\} dt_\tau + \sqrt{2 \left(\frac{1-t_\tau}{\sigma_{t_\tau}^2 t_\tau} \right)} dB_{t_\tau} \\ &= \left\{ \frac{1-t_\tau}{t_\tau \sigma_{t_\tau}^2} \overleftarrow{Y}_\tau + 2 \left(\frac{1-t_\tau}{t_\tau \sigma_{t_\tau}^2} \right) s_{t_\tau}^\leftarrow(\overleftarrow{Y}_\tau) \right\} \times \beta(N-\tau) \times \frac{t_\tau \sigma_{t_\tau}^2}{1-t_\tau} d\tau + \sqrt{2 \left(\frac{1-t_\tau}{\sigma_{t_\tau}^2 t_\tau} \right)} \times \sqrt{\beta(N-\tau) \times \frac{t_\tau \sigma_{t_\tau}^2}{1-t_\tau}} d\overleftarrow{B}_\tau \\ &= \beta(N-\tau) \left\{ \overleftarrow{Y}_\tau + 2s_\tau^\leftarrow(\overleftarrow{Y}_\tau) \right\} d\tau + \sqrt{2\beta(N-\tau)} d\overleftarrow{B}_\tau \\ &= \beta(N-\tau) \left\{ \overleftarrow{Y}_\tau + 2\nabla \log q_{N-\tau}(\overleftarrow{Y}_\tau) \right\} d\tau + \sqrt{2\beta(N-\tau)} d\overleftarrow{B}_\tau, \end{aligned}$$

where $\left\{ \overleftarrow{B}_\tau \right\}_{\tau \geq 0}$ is another Brownian motion.

Initial condition check: Recall that $\overleftarrow{Y}_0 = \frac{\sqrt{\omega_N} \tilde{Z}_{t(N)}}{t(N)} = (\sqrt{\omega_N} + \sqrt{1-\omega_N}) \tilde{Z}_{t(N)}$. Therefore, we have

$$\text{Law}(\overleftarrow{Y}_0) = \text{Law} [(\sqrt{\omega_N} + \sqrt{1-\omega_N}) \cdot \{t(N)X_1 + (1-t(N))X_0\}] = \text{Law}(\sqrt{\omega_N} X_1 + \sqrt{1-\omega_N} X_0) = \text{Law}(Y'_N).$$

This shows that \overleftarrow{Y}_τ satisfies SDE (12).

SDE (12) to SDE (6):

For the other direction, we let $\left\{ \overleftarrow{Y}_\tau \right\}_{\tau \geq 0}$ be a solution of SDE (12). Now, to generate a solution of SDE (6), we need to define

$$\tilde{Z}_t = \frac{t(N-\tau(t)) \overleftarrow{Y}_{\tau(t)}}{\sqrt{\omega_{N-\tau(t)}}} = \frac{\overleftarrow{Y}_{\tau(t)}}{\sqrt{\omega_{N-\tau(t)}} + \sqrt{1-\omega_{N-\tau(t)}}},$$

where $\tau(t)$ should satisfy the following:

$$\begin{aligned}
t(N - \tau(t)) &= \frac{\sqrt{\omega_{N-\tau(t)}}}{\sqrt{\omega_{N-\tau(t)}} + \sqrt{1 - \omega_{N-\tau(t)}}} = t \\
\Rightarrow \omega_{N-\tau(t)} &= \frac{t^2}{t^2 + (1-t)^2} \\
\Rightarrow \exp\left(-2 \int_0^{N-\tau(t)} \beta(u) du\right) &= \frac{t^2}{t^2 + (1-t)^2} \\
\Rightarrow \int_0^{N-\tau(t)} \beta(u) du &= \log\left(\sqrt{1 + \frac{(1-t)^2}{t^2}}\right).
\end{aligned} \tag{53}$$

This shows that $\tilde{Z}_t = \sigma_t \overleftarrow{Y}_{\tau(t)}$. Additionally, (14) yields that the score of \tilde{Z}_t is $s_t(\cdot)$. Now, for convenience, we now write τ to denote $\tau(t)$. Taking derivative w.r.t. t on both sides of (53) yields

$$\frac{d\tau}{dt} = \frac{1}{\beta(N - \tau)} \cdot \frac{(1-t)}{t\sigma_t^2}.$$

Using these facts, we finally get

$$\begin{aligned}
d\tilde{Z}_t &= \frac{(2t-1)}{\sigma_t} \overleftarrow{Y}_\tau + \sigma_t d\overleftarrow{Y}_\tau \\
&= \frac{(2t-1)}{\sigma_t^2} \tilde{Z}_t + \sigma_t \left\{ \overleftarrow{Y}_\tau + 2s_\tau^\leftarrow(\overleftarrow{Y}_\tau) \right\} \beta(N - \tau) d\tau + \sigma_t \sqrt{2\beta(N - \tau)} d\tilde{B}_\tau \\
&= \frac{(2t-1)}{\sigma_t^2} \tilde{Z}_t + \sigma_t \left\{ \frac{\tilde{Z}_t}{\sigma_t} + 2\sigma_t s_t(\tilde{Z}_t) \right\} \frac{(1-t)}{t\sigma_t^2} dt + \sqrt{2 \left(\frac{1-t}{t} \right)} d\tilde{B}_t \\
&= \left(\frac{2t-1}{\sigma_t^2} + \frac{1-t}{t\sigma_t^2} \right) \tilde{Z}_t + 2 \left(\frac{1-t}{t} \right) s_t(\tilde{Z}_t) + \sqrt{2 \left(\frac{1-t}{t} \right)} d\tilde{B}_t \\
&= \frac{\tilde{Z}_t}{t} + 2 \left(\frac{1-t}{t} \right) s_t(\tilde{Z}_t) + \sqrt{2 \left(\frac{1-t}{t} \right)} d\tilde{B}_t.
\end{aligned}$$

Therefore, we \tilde{Z}_t satisfies SDE (6).

C.3. Proof of Proposition 3.5

Recall that $\frac{\tilde{I}_{\theta(s)}}{a_{\theta(s)}} = X_1 + W_{r_{\theta(s)}^2}$, where $r_{\theta(s)}^2 = 1/s$. Now, we define $\hat{U}_s := \frac{\tilde{I}_{\theta(s)}}{a_{\theta(s)}}$. Then, we have $s\hat{U}_s = sX_1 + sW_{1/s}$. Similar to the proofs of Lemma 3.2 and Lemma 3.3, the process $\{\hat{W}_s\}_{s \geq 0} := \{sW_{1/s}\}_{s \geq 0}$ is also a Brownian motion. This finishes the proof by the description of the SL process in (9).

D. Auxiliary results

D.1. Controlling posterior covariance of RF

We recall the SL process (9) to study the dynamics of the conditional covariance matrix $\Sigma_t := \text{Cov}_{1|t}(X_t)$ where $X_t = tX_1 + (1-t)X_0$ and $X_0 \sim N(0, I_d)$. Note that Σ_t is a random matrix. Recall the defintion of \tilde{X}_t in (13). It is evident that $\tilde{\Sigma}_t := \text{Cov}_{1|t}(\tilde{X}_t) \stackrel{d}{=} \Sigma_t$. Due to Lemma 3.3, the SL process (9) is equivalent to the process (13) under time change $t(s) := \frac{\sqrt{s}}{1+\sqrt{s}}$. Then, one can substitute this in Lemma 3.1 to get the following result:

Lemma D.1. *for $t \in [0, 1]$, we have $\frac{d}{dt} \mathbb{E}(\Sigma_t) = -\frac{2t}{(1-t)^3} \mathbb{E}(\Sigma_t^2)$.*

As mentioned in previous section, the above result allows to control the discretization error of the ODE and SDE sampler of RF. More concretely, Lemma D.1 allows us to bound the spectra of Σ_t^2 in terms of the spectra of Σ_t , thereby producing tighter bounds for convergence rate.

D.2. Proof of Proposition B.2

We recall the definitions of $(\mathbf{A}_s)_{s \geq 0}$ and $(\tilde{\Sigma}_{t(s)})_{s \geq 0}$ in Section 3 and Section D.1. Note that $(\mathbf{A}_s)_{s \geq 0}$ and $(\tilde{\Sigma}_{t(s)})_{s \geq 0}$ (see Section 3 and D.1) are also equivalent in law. This is simply due to the fact that $\tilde{\Sigma}_{t(s)} = \text{Cov}_{1|t(s)}(\tilde{X}_{t(s)}) = \text{Cov}_{1|t(s)}(s\tilde{X}_{t(s)}/t(s))$, and the distributional equivalence of the two processes $(U_s)_{s \geq 0}$ and $(s\tilde{X}_{t(s)}/t(s))_{s \geq 0}$. It is known that the random matrix valued process $(\mathbf{A}_s)_{s \geq 0}$ obeys the following SDE:

$$d\mathbf{A}_s = -\mathbf{A}_s^2 ds + \mathcal{M}_s^{(3)} dB_s, \quad (54)$$

where $\mathcal{M}_s^{(\ell)} = \mathbb{E}[(X_1 - \mathbb{E}[X_1 | U_s])^{\otimes \ell} | U_s]$. More details on this can be found in (Eldan, 2020, Section 4.2.1) or (Alberts et al., 2025, Section 3). Since the two processes $(\mathbf{A}_s)_{s \geq 0}$ and $(\tilde{\Sigma}_{t(s)})_{s \geq 0}$ are equivalent in law, SDE (54) immediately yields

$$d\tilde{\Sigma}_t = -\frac{2t}{(1-t)^3} \tilde{\Sigma}_t^2 dt + \tilde{\mathcal{M}}_t^{(3)} dB_{t^2/(1-t)^2}, \quad (55)$$

where $\tilde{\mathcal{M}}_t^{(\ell)} = \mathbb{E}[(X_1 - \mathbb{E}[X_1 | \tilde{X}_t])^{\otimes \ell} | \tilde{X}_t]$. Now, an application of Ito's formula on (54) yields

$$d(\text{Trace}(\mathbf{A}_s^2)) = -2 \langle \mathbf{A}_s, \mathbf{A}_s^2 \rangle ds + \langle \mathcal{M}_s^{(3)}, \mathcal{M}_s^{(3)} \rangle ds + 2 \langle \mathbf{A}_s, \mathcal{M}_s^{(3)} \rangle dB_s$$

Taking expectation on both side we arrive at the following inequality:

$$d(\text{Trace}[\mathbb{E}(\mathbf{A}_s^2)]) = -2\mathbb{E}[\langle \mathbf{A}_s, \mathbf{A}_s^2 \rangle] ds + \mathbb{E}[\langle \mathcal{M}_s^{(3)}, \mathcal{M}_s^{(3)} \rangle] ds.$$

Finally, using the fact that \mathbf{A}_s and $\Sigma_{t(s)}$ have the same law, chain rule yields the following:

$$d(\text{Trace}[\mathbb{E}(\Sigma_t^2)]) = -\frac{4t}{(1-t)^3} \mathbb{E}[\langle \Sigma_t, \Sigma_t^2 \rangle] dt + \frac{2t}{(1-t)^3} \mathbb{E}[\langle \tilde{\mathcal{M}}_t^{(3)}, \tilde{\mathcal{M}}_t^{(3)} \rangle] dt. \quad (56)$$

We first focus on the first term on the right-hand side of (56). Using the symmetry of Σ_t , we observe that

$$\begin{aligned} \mathbb{E}[\langle \Sigma_t, \Sigma_t^2 \rangle] &= \mathbb{E}[\text{Trace}(\Sigma_t^3)] \\ &\leq \mathbb{E}[\|\Sigma_t\|_{\text{op}} \|\Sigma_t\|_F^2] \\ &= \mathbb{E}[\text{Trace}(\Sigma_t) \|\Sigma_t\|_F^2] \\ &= \mathbb{E}[\text{Trace}(\Sigma_t) \mathbb{1}\{X_t \in \mathcal{T}_t\} \|\Sigma_t\|_F^2] + \mathbb{E}[\text{Trace}(\Sigma_t) \mathbb{1}\{X_t \notin \mathcal{T}_t\} \|\Sigma_t\|_F^2] \\ &\leq C_3 \frac{(1-t)^2}{t^2} (k \log N) \mathbb{E}[\|\Sigma_t\|_F^2] + \mathbb{E}[\text{Trace}(\Sigma_t) \mathbb{1}\{X_t \notin \mathcal{T}_t\} \|\Sigma_t\|_F^2], \end{aligned} \quad (57)$$

where the last inequality follows due to (37). Regarding the last term in above display, Assumption 4.2 and (36) yields

$$\mathbb{E}[\text{Trace}(\Sigma_t) \mathbb{1}\{X_t \notin \mathcal{T}_t\} \|\Sigma_t\|_F^2] \leq 8N^{3c_R} \mathbb{P}(X_t \notin \mathcal{T}_t) \leq \frac{1}{N^{10}}.$$

Therefore, we arrive at

$$\mathbb{E}[\langle \Sigma_t, \Sigma_t^2 \rangle] \leq C_3 \frac{(1-t)^2}{t^2} (k \log N) \mathbb{E}[\|\Sigma_t\|_F^2] + \frac{1}{N^{10}}. \quad (58)$$

Substituting this in (57) yields,

$$\begin{aligned} d\mathbb{E}(\|\Sigma_t\|_F^2) &= -\frac{4t}{(1-t)^3} \mathbb{E}[\langle \Sigma_t, \Sigma_t^2 \rangle] dt + \frac{2t}{(1-t)^3} \mathbb{E}[\langle \tilde{\mathcal{M}}_t^{(3)}, \tilde{\mathcal{M}}_t^{(3)} \rangle] dt \\ &\geq -\frac{4t}{(1-t)^3} \mathbb{E}[\langle \Sigma_t, \Sigma_t^2 \rangle] dt \\ &\geq -\frac{4C_3 k \log N}{(1-t)t} \mathbb{E}[\|\Sigma_t\|_F^2] dt - \frac{4t}{(1-t)^3} \cdot \frac{1}{N^{10}} dt \\ &\geq -\frac{4C_3 k \log N}{(1-t_i)t_{i-1}} \mathbb{E}[\|\Sigma_t\|_F^2] dt - \frac{4t_i}{(1-t_i)^3} \cdot \frac{1}{N^{10}} dt, \end{aligned}$$

where the last line follows holds provided $t \in [t_{i-1}, t_i]$ with $i > 1$. Therefore, we can conclude that

$$\begin{aligned} & \exp \left\{ \frac{4C_3 k t \log N}{(1-t_i)t_{i-1}} \right\} \mathbb{E}(\|\Sigma_t\|_F^2) - \exp \left\{ \frac{4C_3 k t_{i-1} \log N}{(1-t_i)t_{i-1}} \right\} \mathbb{E}(\|\Sigma_{t_{i-1}}\|_F^2) \\ & \geq -\frac{4t_i}{(1-t_i)^3} \cdot \frac{1}{N^{10}} \int_{t_{i-1}}^t \exp \left\{ \frac{4C_3 k t \log N}{(1-t_i)t_{i-1}} \right\} dt \\ & \geq -\frac{t_i t_{i-1}}{C_3 k (1-t_i)^2 \log N} \cdot \frac{1}{N^{10}} \left(\exp \left\{ \frac{4C_3 k t \log N}{(1-t_i)t_{i-1}} \right\} - \exp \left\{ \frac{4C_3 k t_{i-1} \log N}{(1-t_i)t_{i-1}} \right\} \right) \end{aligned}$$

Dividing both sides by $\exp \left\{ \frac{4C_3 k t_{i-1} \log N}{(1-t_i)t_{i-1}} \right\}$, we obtain

$$\begin{aligned} & \exp \left\{ \frac{4C_3 k (t - t_{i-1}) \log N}{(1-t_i)t_{i-1}} \right\} \mathbb{E}(\|\Sigma_t\|_F^2) - \mathbb{E}(\|\Sigma_{t_{i-1}}\|_F^2) \\ & \geq -\frac{t_i t_{i-1}}{C_3 k (1-t_i)^2 \log N} \cdot \frac{1}{N^{10}} \left(\exp \left\{ \frac{4C_3 k (t - t_{i-1}) \log N}{(1-t_i)t_{i-1}} \right\} - 1 \right) \\ & \geq -\frac{1}{C_3 k (1-t_i)^2 \log N} \cdot \frac{1}{N^{10}} \left(\exp \left\{ \frac{4C_3 k (t - t_{i-1}) \log N}{(1-t_i)t_{i-1}} \right\} - 1 \right). \end{aligned}$$

Now, recall that $\frac{\eta_{t_i}}{(1-t_i)t_i} \leq 2h$. Using this inequality coupled with (16) gives us

$$\frac{4C_3 k (t - t_{i-1}) \log N}{(1-t_i)t_{i-1}} \leq \frac{4C_3 k \eta_{t_{i-1}} \log N}{(1-t_i)t_{i-1}} \leq 8C_3 k h \log N < 1,$$

provided N is sufficiently large. Therefore, we have

$$\begin{aligned} \mathbb{E}(\|\Sigma_{t_{i-1}}\|_F^2) & \leq \exp \left\{ \frac{4C_3 k (t - t_{i-1}) \log N}{(1-t_i)t_{i-1}} \right\} \mathbb{E}(\|\Sigma_t\|_F^2) \\ & \quad + \frac{1}{C_3 k (1-t_i)^2 \log N} \cdot \frac{1}{N^{10}} \left(\exp \left\{ \frac{4C_3 k (t - t_{i-1}) \log N}{(1-t_i)t_{i-1}} \right\} - 1 \right) \\ & \leq 3\mathbb{E}(\|\Sigma_t\|_F^2) + \frac{24h}{(1-t_i)^2 N^{10}}. \end{aligned}$$

The inequality follows from $e^x - 1 \leq x$ for $x \in (0, 1)$, and $\frac{\eta_{t_i}}{(1-t_i)t_i} \leq 2h$. Substituting t_{i-1} by t_i in the above inequality, we get the following

$$\mathbb{E}(\|\Sigma_{t_i}\|_F^2) \leq 3\mathbb{E}(\|\Sigma_t\|_F^2) + \frac{24h}{(1-t_{i+1})^2 N^{10}}, \quad t \in [t_i, t_{i+1}], i \geq 1.$$

Now we use Lemma D.1 to get

$$\begin{aligned} \mathbb{E}[\text{Trace}(\Sigma_{t_{i+1}})] - \mathbb{E}[\text{Trace}(\Sigma_{t_i})] & = - \int_{t_i}^{t_{i+1}} \frac{2t}{(1-t)^3} \mathbb{E}(\|\Sigma_t\|_F^2) \\ & \leq - \int_{t_i}^{t_{i+1}} \frac{2t}{3(1-t)^3} \mathbb{E}(\|\Sigma_{t_i}\|_F^2) dt + \frac{8h\eta_{t_i}}{(1-t_{i+1})^2 N^{10}} \\ & \leq - \frac{2\eta_{t_i}(t_{i+1} + t_i)}{3(1-t_{i+1})^2(1-t_i)^2} \mathbb{E}(\|\Sigma_{t_i}\|_F^2) + \frac{8h\eta_{t_i}}{(1-t_{i+1})^2 N^{10}} \end{aligned}$$

Rearranging the terms in the above inequality and using $t_{i+1} + t_i > 2t_i$, we finally get

$$\frac{\eta_{t_i} t_i}{(1-t_{i+1})^2(1-t_i)^2} \mathbb{E}(\|\Sigma_{t_i}\|_F^2) \leq \frac{3}{4} (\mathbb{E}[\text{Trace}(\Sigma_{t_i})] - \mathbb{E}[\text{Trace}(\Sigma_{t_{i+1}})]) + \frac{6h\eta_{t_i}}{(1-t_{i+1})^2 N^{10}}. \quad (59)$$

D.3. Proof of Claim (38)

Lemma D.2. *Let $t_{i+1} = t_i + \eta_i$ with $0 < t_i \leq t_{i+1} \leq 1$. Then*

$$\frac{(1-t_i)^2}{t_i^2} - \frac{(1-t_{i+1})^2}{t_{i+1}^2} \leq \frac{2\eta_i}{t_i^3}.$$

Proof. Define $f(t) := \frac{(1-t)^2}{t^2}$ for $t > 0$. A direct calculation gives

$$f'(t) = \frac{2(t-1)}{t^3}.$$

By the mean value theorem, there exists $\xi \in (t_i, t_{i+1})$ such that

$$f(t_i) - f(t_{i+1}) = -f'(\xi)(t_{i+1} - t_i) = \frac{2(1-\xi)}{\xi^3} \eta_i.$$

Since $\xi \geq t_i$ and $\xi \leq 1$, we have $(1-\xi)/\xi^3 \leq 1/t_i^3$, which implies the desired bound. \square